Stress induces dynamic, cytotoxicity-antagonizing TDP-43 nuclear bodies via paraspeckle lncRNA *NEAT1*-mediated liquid-liquid phase separation

Chen Wang[1,2,4], Yongjia Duan[1,2,4], Gang Duan[1,2,4], Qiangqiang Wang[1], Kai Zhang[1,2], Xue Deng[1,2], Beituo Qian[1,2], Jinge Gu[1,2], Zhiwei Ma[1,5], Shuang Zhang[1], Lin Guo[3], Cong Liu[1,2,*], and Yanshan Fang[1,2,6,*]

[1]Interdisciplinary Research Center on Biology and Chemistry, Shanghai Institute of Organic Chemistry, Chinese Academy of Sciences, Shanghai 201210, China

[2]University of Chinese Academy of Sciences, Beijing, 100049, China,

[3]Department of Biochemistry and Molecular Biology, Thomas Jefferson University, Philadelphia, PA 19107, USA

[4]These authors contributed equally

[5]Current address: West China School of Basic Medical Sciences and Forensic Medicine, Sichuan University, Chengdu, 610041, China

[6]Lead Contact

***Correspondence to**:

Cong Liu: liulab@sioc.ac.cn

Yanshan Fang: fangys@sioc.ac.cn

Tel: +86-21-6858.2510

Fax: +86-21-6858.2502

Short title (<50 characters): Phase-separated TDP-43 NBs mitigate stress

Keywords: TDP-43; nuclear body; phase separation; lncRNA *NEAT1*; ALS

***Word count**: ~8400 words (excluding the title page, graphic abstract, methods and reference)*

Graphic Abstract

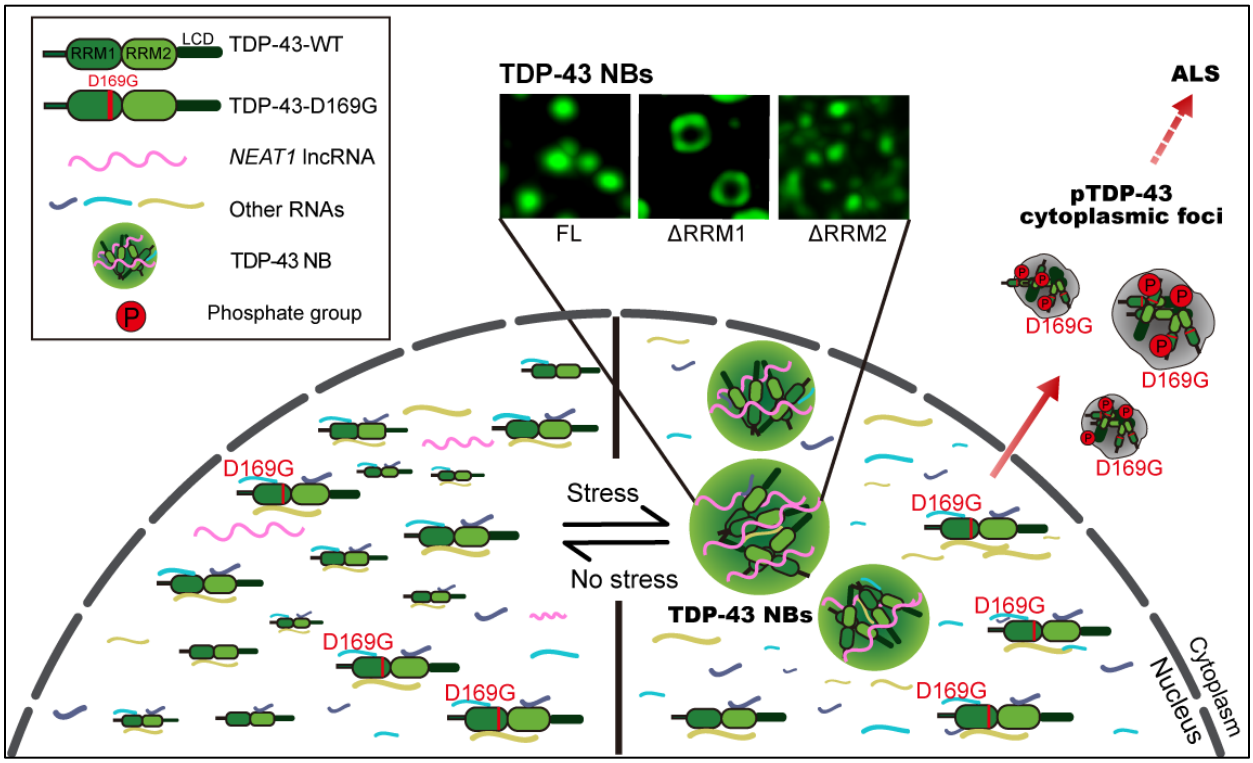

Highlights *(Up to four bullet points. The length of each highlight cannot exceed 85 characters, including spaces)*

- Stress induces phase-separated TDP-43 NBs to alleviate cytotoxicity
- The two RRMs interact with different RNAs and act distinctly in the assembly of TDP-43 NBs
- LncRNA *NEAT1* promotes TDP-43 LLPS and is upregulated in stressed neurons
- The ALS-causing D169G mutation is NB-defective and forms pTDP-43 cytoplasmic foci

SUMMARY (< 150 words)

Despite the prominent role of TDP-43 in neurodegeneration, its physiological and pathological functions are not fully understood. Here, we report an unexpected function of TDP-43 in the formation of dynamic, reversible, liquid droplet-like nuclear bodies (NBs) in response to stress. Formation of NBs alleviates TDP-43-mediated cytotoxicity in mammalian cells and fly neurons. Super-resolution microscopy reveals a “core-shell” organization of TDP-43 NBs, antagonistically maintained by the two RRMs. TDP-43 NBs are partially colocalized with nuclear paraspeckles, whose scaffolding lncRNA *NEAT1* is dramatically upregulated in stressed neurons. Moreover, increase of *NEAT1* promotes TDP-43 liquid-liquid phase separation (LLPS) *in vitro*. Finally, we uncover that the ALS-associated mutation D169G impairs the *NEAT1*-mediated TDP-43 LLPS and NB assembly, causing excessive cytoplasmic translocation of TDP-43 to form stress granules that become phosphorylated TDP-43 cytoplasmic foci upon prolonged stress. Together, our findings suggest a stress-mitigating role and mechanism of TDP-43 NBs, whose dysfunction may be involved in ALS pathogenesis.

45 **INTRODUCTION**

46 Amyotrophic lateral sclerosis (ALS) is a progressive motor neuron disease characterized by the
47 degeneration of motor neurons in the brain and spinal cord, which leads to fatal paralysis
48 generally within 2–5 years after diagnosis (Taylor et al., 2016; van Es et al., 2017). Missense
49 mutations in the gene *TARDBP* encoding the trans-activation response element (TAR)
50 DNA-binding protein 43 (TDP-43) predispose to familial ALS, and cytoplasmic protein inclusions
51 containing pathologically phosphorylated and ubiquitinated TDP-43 in motor neurons are a
52 pathological hallmark of ALS (Neumann et al., 2006; Kabashi et al., 2008). TDP-43 is a nuclear
53 protein but can shuttle between the nucleus and the cytoplasm. It has a nuclear localization
54 signal (NLS), a nuclear export signal (NES), two canonical RNA recognition motifs (RRMs) that
55 bind to nucleic acids, and a C-terminal low complexity domain (LCD) that mediates
56 protein-protein interactions and is enriched of disease-associated mutations (Kabashi et al.,
57 2008; Lee et al., 2012). TDP-43 is engaged in a variety of ribonucleoprotein (RNP) complexes
58 and plays an important role in RNA processing and homeostasis (Jovičić et al., 2016; Ratti and
59 Buratti, 2016; Ederle and Dormann, 2017; Fahrenkrog and Harel, 2018; Zhao et al., 2018). In
60 addition, TDP-43 is known to participate in cytoplasmic stress granules (SGs), which may
61 undergo aberrant phase transition and promote the formation of solid protein aggregates in
62 diseased conditions (Li et al., 2013; Ramaswami et al., 2013; Murakami et al., 2015; Patel et al.,
63 2015).

64 Nuclear bodies (NBs) are dynamic, membraneless nuclear structures that concentrate
65 specific nuclear proteins and RNAs and play an important role in maintaining nuclear
66 homeostasis and RNA processing (Stanek and Fox, 2017; Wegener and Müller-McNicoll, 2018).
67 Increasing evidence suggests the association of TDP-43 with a variety of NBs, such as
68 paraspeckles (Dammer et al., 2012; Nishimoto et al., 2013; West et al., 2016), gemini of coiled
69 bodies (GEMs) (Ishihara et al., 2013), nuclear stress bodies (Udan-Johns et al., 2014),
70 interleukin-6 and -10 splicing activating compartment bodies (InSAC bodies) (Lee et al., 2015),
71 and omega speckles (Piccolo et al., 2018). Notably, in the nucleus of spinal motor neurons of

72 sporadic ALS patients, TDP-43 is found colocalized with paraspeckles and the occurrence of
73 paraspeckles is specifically increased in the early phase of the disease (Nishimoto et al., 2013).
74 Excessive formation of dysfunctional paraspeckles is also observed in motor neurons of
75 ALS-FUS patients (An et al., 2019). Paraspeckles are a class of subnuclear RNP granules
76 formed by the scaffolding lncRNA *NEAT1* associated with splicing factor proline-glutamine rich
77 (SFPQ), P54NRB/NONO and other paraspeckle proteins, which are engaged in regulating
78 cellular functions through nuclear retention of mRNAs and proteins (Bond and Fox, 2009; Fox
79 and Lamond, 2010; Nakagawa et al., 2018). Although TDP-43 is present in NBs such as
80 paraspeckles that sometimes accompany neurodegeneration, our understanding about the
81 function of TDP-43 in NBs and the involvement of NBs in ALS pathogenesis is still rudimentary.

82 Recent studies indicate that liquid-liquid phase separation (LLPS) of RNA-binding protein
83 (RBPs) drives the assembly of liquid droplet (LD)-like, membraneless RNP granules in the
84 cytoplasm and nucleoplasm (Lin et al., 2015; Feric et al., 2016; Banani et al., 2017; Uversky,
85 2017; Nakagawa et al., 2018; Fox et al., 2018). Several ALS-related RBPs including TDP-43,
86 FUS, hnRNP A1, hnRNP A2 and TIA1 are shown to phase separate *in vitro* (Hyman et al., 2014;
87 Molliex et al., 2015; Patel et al., 2015; Schmidt and Rohatgi, 2016; Mackenzie et al., 2017; Ryan
88 et al., 2018; Wang et al., 2018). The intrinsically disordered LCD domains of the RBPs are
89 thought to mediate the LLPS (Hennig et al., 2015; Molliex et al., 2015; Xiang et al., 2015; Murray
90 et al., 2017; Uversky, 2017) and posttranslational protein modifications play an important role in
91 determining the biophysical and biological properties of the phase behavior of the RBPs (Brady
92 et al., 2011; Cohen et al., 2015; Li et al., 2017; Hofweber et al., 2018; Luo et al., 2018; McGurk et
93 al., 2018; Qamar et al., 2018; Ryan et al., 2018; Duan et al., 2019). In addition to the LCD, recent
94 studies reveal that RNA is of vital importance in regulating the LLPS (Dominguez et al., 2018;
95 Namkoong et al., 2018; Fox et al., 2018), which can either suppress or promote phase
96 separation depending on the contents and concentrations of the RNAs (Shevtsov and Dundr,
97 2011; Lin et al., 2015; Maharana et al., 2018; Mann et al., 2019).

98 In this study, we find that various cellular stresses induce TDP-43 to form distinct, highly

99 dynamic and reversible NBs, which not only attenuate the cytotoxicity of TDP-43 in mammalian
100 cells but also ameliorate neurodegeneration and behavioral deficits in a *Drosophila* model of ALS.
101 Further investigation with super-resolution microscopy uncovers the distinct functions of the two
102 RRMs in maintaining the morphology and size of TDP-43 NBs. Moreover, we reveal a crucial
103 role of the paraspeckle scaffolding long non-coding RNA (lncRNA) nuclear-enriched abundant
104 transcript 1 (*NEAT1*) in promoting TDP-43 LLPS, which is compromised by the ALS-causing
105 mutation D169G and causes a defect in TDP-43 NB formation. The NB-forming defective D169G
106 mutant is prone to accumulate disease hallmarked, hyperphosphorylated TDP-43 foci in the
107 cytoplasm with prolonged stress. Together, our findings propose that stress induces the
108 assembly of TDP-43 NBs in the generally "suppressive" nucleoplasm environment via
109 upregulation of lncRNA *NEAT1* which promotes TDP-43 LLPS, and the defective
110 stress-mitigating TDP-43 NBs may contribute to ALS pathogenesis.
111

112 **RESULTS**

113 **Arsenic stress induces dynamic and reversible TDP-43 NBs**

114 TDP-43 protein is predominantly localized to the nucleus but can shuttle between the nucleus
115 and the cytoplasm. In response to cellular stress, TDP-43 is recruited to cytoplasmic SGs (Li et
116 al., 2013). Interestingly, in an earlier related work of our group (Duan et al., 2019), we noticed
117 that although arsenite, a commonly used reagent to raise cellular stress (Bernstam and Nriagu,
118 2000), induced TDP-43$^+$ cytoplasmic SGs, the majority of TDP-43 signal remained in the nucleus.
119 More than that, in a higher percentage of the cells, nuclear TDP-43 lost the normal diffused
120 pattern and instead exhibited a distinct granular appearance (Figures 1A and 1B, and Movie S1).
121 Similarly, endogenous TDP-43 also formed granules in the nucleus upon arsenic stress (Figures
122 1C and 1D), with the size ranging from 0.01 to 0.67 μm^2 and the median average of 0.019 μm^2
123 (Figure 1E).

124 A membraneless nuclear structure fulfills the requirements of NBs if it is: (1) microscopically
125 visible, (2) enriched with specific nuclear factors, and (3) continuously exchanging the contents
126 with the surrounding nucleoplasm (Stanek and Fox, 2017). Indeed, arsenite-induced TDP-43
127 nuclear granules were microscopically visible (Figures 1A-1E). Further examination by
128 immunocytochemistry indicated that these arsenite-induced nuclear granules were colocalized
129 or partially colocalized with several known types of NBs, especially paraspeckles labeled by
130 SFPQ (Figure S1). Thus, the stress-induced TDP-43 nuclear granules were enriched of not only
131 TDP-43 but also other nuclear factors such as paraspeckle proteins.

132 To examine if stress-induced TDP-43 nuclear granules were LD-like and could exchange
133 with surrounding nucleoplasm, we performed the fluorescence recovery after photobleaching
134 (FRAP) analysis in *live* cells using a green fluorescent protein (GFP)-tagged TDP-43
135 (GFP-TDP-43). To induce TDP-43 nuclear granules, cells were pre-treated with arsenite (250 μM)
136 for 30 minutes before photobleaching. The fluorescence of GFP-TDP-43 nuclear granules was
137 rapidly recovered after photobleaching, reaching ~50% of the pre-bleaching intensity in ~65
138 seconds (Figures 1F and 1H, and Movie S2), indicating that stress-induced TDP-43 nuclear
139 granules are LD-like and highly dynamic. Together, they fulfill all the above three requirements
140 and are thereafter called TDP-43 NBs in this study.

141 Next, we determined whether stress-induced TDP-43 NBs were reversible. In the arsenite
142 washout assay, stress-induced TDP-43 NBs gradually disappeared and eventually recovered to
143 nearly diffused pattern similar to that before the arsenite treatment (Figure 1I). Our quantitative
144 analyses indicated that both the percentages of cells with TDP-43 NBs and the number of
145 TDP-43 NBs per cell decreased in a time-dependent manner after arsenite washout (Figures
146 1J-1L). Thus, the arsenic stress-induced TDP-43 NBs are reversible. With prolonged stress such
147 as the arsenite treatment (250 μM) for 6 h, the TDP-43 NBs were no longer dynamic and did not
148 rapidly recover after photobleaching (Figures 1G and 1H).

149

150 **Formation of TDP-43 NBs as a general cellular stress mechanism**

151 It was reported that TDP-43 formed reversible nuclear "aggregation" during heat shock
152 (Udan-Johns et al., 2014), which together with the above arsenite-induced TDP-43 NBs raised
153 the possibility that the assembly of TDP-43 NBs might be a general mechanism employed by the
154 nucleus in response to stress. Consistent with this idea, we found that disturbing the nuclear
155 homeostasis by inhibition of nuclear export with leptomycin B (LMB) also induced endogenous
156 TDP-43 to form NBs (Figures 2A and 2B). Hence, as induced by arsenic stress (Figures 1C-1E),
157 the formation of TDP-43 NBs was not an artificial effect simply due to TDP-43 overexpression.

158 To determine whether blocking the nuclear export of TDP-43 itself was sufficient to induce
159 the formation of TDP-43 NBs, we generated the NLS and NES mutants of TDP-43, namely
160 NLS^{mut} and NES^{mut} (Figure 2C). Under normal conditions, wild-type (WT) TDP-43 was largely
161 diffused in the nucleus with rare occurrence of spontaneous TDP-43 NBs (Figures 2D-2F). As
162 expected, TDP-43-NLS^{mut} was predominantly cytoplasmic and thus the chance of the NLS^{mut} to
163 form NBs was even lower than that of WT TDP-43 (Figures 2D and 2E). In contrast, the NES^{mut}
164 was exclusively nuclear and formed TDP-43 NBs even in the absence of stress (Figures 2D-2F).
165 Furthermore, the solubility of TDP-43-NES^{mut} protein was significantly reduced, as more than half
166 of TDP-43-NES^{mut} protein was insoluble in radioimmunoprecipitation assay buffer (RIPA)
167 (Figures 2G and 2H). Of note, the total protein levels (the sum of the soluble and insoluble
168 fractions) of NLS^{mut} and NES^{mut} are not statistically different from that of WT TDP-43 (p = 0.8451
169 and 0.2835, respectively; one-way ANOVA).

170 The marked reduction in the solubility of the NES^{mut} protein raised the question whether the
171 TDP-43-NES^{mut} NBs were still in a dynamic, LD-like state or had become solid aggregation. First,
172 we performed the FRAP assay in *live* cells, which indicated that the NES^{mut} NBs were dynamic,
173 as the fluorescence signal of GFP-TDP-43NES^{mut} rapidly recovered after photobleaching, just
174 like the phenotype of the known nuclear body protein SFPQ (Figures S2A-S2B). Next, we
175 examined the stability of WT and mutant TDP-43 by treating cells with protein synthesis inhibitor
176 cycloheximide (CHX). We found that the RIPA-soluble TDP-43 protein was rather stable, as
177 none of WT, NLS^{mut} or NES^{mut} TDP-43 in the soluble fractions showed significant turnover in 24 h

178 after CHX treatment (Figures S2C-S2F). In contrast, the RIPA-insoluble fraction of
179 TDP-43-NES^{mut} decreased rapidly upon CHX inhibition and became almost undetectable within
180 24 h (Figures S2C-S2F). Meanwhile, the CHX treatment led to disassembly of TDP-43-NES^{mut}
181 NBs (Figures S2G and S2H). These results suggest that the RIPA-insoluble TDP-43-NES^{mut} NBs
182 were dynamic and reversible, and therefore they were not "protein aggregates" as ones might
183 presumed based on their punctate morphology and the detergent-insolubility. Of note, a recent
184 study reported that stress promoted misfolded proteins to enter the phase-separated, LD-like
185 nucleolus, which might function as a protein quality control mechanism in the nucleus (Frottin et
186 al., 2019).

187 Next, we examined how disturbance of the cellular proteostasis impacted on TDP-43 NBs by
188 inhibition of proteasome-mediated protein degradation with MG132. It led to a significant
189 increase in the RIPA-insoluble fraction of NES^{mut} as well as WT TDP-43 protein (Figures
190 S2I-S2L). In contrast, blocking autophagic flux with chloroquine (CQ) did not significantly affect
191 the levels of insoluble TDP-43 (Figures S2M-S2P). Thus, unlike misfolded protein aggregates,
192 the turnover of TDP-43 NBs did not rely on the autophagy-lysosomal pathway. Together, TDP-43
193 NBs are distinct from protein aggregates. Instead, they are dynamic, reversible membraneless
194 subnuclear organelles that are sensitive and rapidly respond to changes in the microenvironment
195 of the nucleoplasm.

196

197 **Formation of TDP-43 NBs alleviates the cytotoxicity in mammalian cells and fly neurons**
198 ***in vivo***

199 We were keen to understand the functional significance of forming TDP-43 NBs in cells. Could it
200 be a cellular "protective" mechanism like SGs? To answer this question, we examined how cells
201 expressing WT, NLS^{mut} or NES^{mut} TDP-43 responded to cellular stress. Compared to WT
202 TDP-43, cells transfected with the NLS^{mut} showed significantly increased cell death indicated by
203 the propidium iodide (PI) staining, whereas the NES^{mut} was more resistant to arsenic stress
204 (Figure S3A-S3D). Furthermore, we examined how the NB formation impacted on TDP-43

205 overexpression (OE)-mediated cytotoxicity *per se*. We found that OE of WT or NLS^{mut} but not
206 NES^{mut} TDP-43 in human 293T cells significantly decreased the cell viability using the cell
207 counting kit-8 (CCK-8) assay (Figure 3A) or by measuring the ATP levels (Figure 3B). These
208 results were consistent with the previous studies that expression of cytoplasmic TDP-43 was
209 more toxic than nuclear TDP-43 in flies (Miguel et al., 2011) and primary rat neurons (Barmada
210 et al., 2010). However, the reduced cytotoxicity of nuclear TDP-43 had not been associated with
211 the formation of NBs before.

212 To confirm whether TDP-43 form NBs *in vivo* and to examine how they impacted on
213 neurodegeneration, we generated transgenic flies to express WT, NLS^{mut} or NES^{mut} human
214 TDP-43 (hTDP-43) by ΦC31 integrase-mediated, site-specific integration (Groth et al., 2003;
215 Bateman et al., 2006). The strains generated by this approach were different from the previously
216 published NLS^{mut} and NES^{mut} hTDP-43 flies (Miguel et al., 2011), as in this study the different
217 UAS-*hTDP-43* transgenes were integrated into the fly genome at the same chromatin locus,
218 which avoided the location effect on the expression levels of the transgenes among different
219 strains and allowed direct comparison between the WT and the mutant TDP-43 flies.
220 Immunohistochemistry analysis of the whole mount fly brains confirmed the predominant nuclear
221 localization of the WT and NES^{mut} hTDP-43 in fly neurons (*elav*-Gal4), whereas the NLS^{mut} was
222 largely cytoplasmic (Figure S4A). Consistent with the data in mammalian cells, the NES^{mut}
223 hTDP-43 formed striking NBs in the nucleus of fly neurons (Figure S4A-S4B) and the solubility
224 was significantly decreased (Figures S4C-S4D). We then examined the consequence of
225 expressing WT, NLS^{mut} or NES^{mut} hTDP-43 in fly eyes to compare the degenerative
226 morphological changes they caused (Figure S4E) and in motor neurons to compare the
227 behavioral decline they induced (Figure S4F). In both experiments, WT TDP-43 flies exhibited
228 marked age-dependent degenerative phenotypes and the NLS^{mut} flies were significantly worse.
229 In contrast, the neurotoxicity of TDP-43-NES^{mut} was substantially milder, especially in the
230 ALS-related functional assay, the climbing capability of the NES^{mut} flies was not statistically
231 different from that of the control flies (UAS-*Luciferase*) at all time points examined (Figure S4F).

232 To further confirm that the formation of TDP-43 NBs was indeed required for the
233 cytotoxicity-antagonizing effect rather than simply restricting TDP-43 in the nucleus, we sought
234 for alternative approaches to induce TDP-43 NBs without disrupting its nucleocytoplasmic
235 transport. Acetylation of TDP-43 at K145 and K192 was previously shown to regulate RNA
236 binding and affect TDP-43 aggregation (Cohen et al., 2015). The acetylation-mimic mutation
237 (K145/192Q) induced whereas the acetylation-deficient mutation (K145/192R) suppressed the
238 formation of TDP-43 protein inclusions (Cohen et al., 2015). Hence, we generated K145/192Q
239 mutation in WT TDP-43 (Figure 3C), which led to the assembly of TDP-43 NBs in the absence of
240 cellular stress (Figures 3E-3E' and 3G). On the other hand, we introduced K145/192R mutation
241 into TDP-43-NES^{mut} (Figure 3D), which abolished the spontaneous TDP-43-NES^{mut} NBs (Figures
242 3F-3F' and 3H). In addition, we confirmed that neither K145/192Q nor K145/192R significantly
243 altered the subcellular distribution of TDP-43 (Figures 3I and 3J). Consistent with our hypothesis,
244 the NB-forming K145/192Q mutation alleviated the cytotoxicity of WT TDP-43 (Figure 3K),
245 whereas K145/192R abolished the NB-forming capability and made the originally non-toxic
246 TDP-43-NES^{mut} to manifest marked cytotoxicity (Figure 3L). Thus, the formation of TDP-43 NBs
247 can mitigate cytotoxicity, which might help cells to survive stressed or diseased conditions.
248

249 **The role of the major functional domains of TDP-43 in the assembly of NBs**

250 We went on to investigate how TDP-43 NBs were assembled. First, to understand the function of
251 each major domain in TDP-43 NB formation, we generated truncated TDP-43, namely ΔLCD,
252 ΔRRM1 and ΔRRM2 (Figure S5A). Both WT and ΔLCD TDP-43 proteins were mostly nuclear
253 and soluble (Figures S5B and S5C); however, ΔLCD did not form NBs in response to stress
254 (Figures S5F to S5G'), confirming a major role of the LCD domain in promoting the assembly of
255 RNP granules and protein aggregation (Molliex et al., 2015; Conicella et al., 2016). Next, we
256 examined the impact of RRM1 or RRM2 on the assembly of TDP-43 NBs. TDP-43-ΔRRM1 was
257 soluble (Figure S5D), whereas ΔRRM2 showed a remarkable increase of insolubility (Figure
258 S5E). More interestingly, TDP-43-ΔRRM1 formed large, ring-shaped structures in the nucleus

259 without any stress (Figure S5H-S5H'); while ΔRRM2 looked similar to WT TDP-43 without stress
260 and showed a grainy appearance with LMB treatment (Figures S5I-S5I').

261 To further characterize the nuclear structures formed by WT, ΔRRM1 and ΔRRM2 TDP-43,
262 we utilized the Leica LIGHTNING SP8 confocal microscope to capture multicolor images in
263 super-resolution down to 120 nm. We found that WT TDP-43 formed solid, mid-size NBs;
264 ΔRRM1 was much larger, ring-shaped; and ΔRRM2 displayed a mesh-like structure with
265 numerous smaller NBs (Figures 4A and 4B). Super-resolution three-dimensional (3D) rendering
266 revealed that WT and ΔRRM2 TDP-43 NBs were mostly in oval or sometimes cylinder shapes,
267 while ΔRRM1 formed large, hollow "pillars". Further measurement of the diameters confirmed
268 that ΔRRM1 "rings" was drastically larger whereas ΔRRM2 NBs was slightly smaller than WT
269 TDP-43 NBs (Figure 4C).

270 Given the distinct morphology of the nuclear structures formed by ΔRRM1 and ΔRRM2
271 TDP-43, it was tempting to propose that TDP-43 NBs, similar to paraspeckles (West et al., 2016),
272 might have a "core-shell" organization (Figure 4D). Moreover, we hypothesized that the two
273 RRMs might function antagonistically to keep the shape and the size of TDP-43 NBs. In other
274 words, the tension maintained by the two RRMs might prevent TDP-43 NBs from expanding
275 unrestrainedly to become huge nuclear bubbles as well as from condensing all into the core to
276 become insoluble aggregates. To test this hypothesis, we co-expressed HA-tagged WT TDP-43
277 with Myc-tagged WT, ΔRRM1 or ΔRRM2 TDP-43 and induced the NB formation in 293T cells by
278 LMB (Figures 4E-4H). The super-resolution images showed that ΔRRM1 formed a ring-shaped
279 shell wrapping the co-expressed WT TDP-43 NBs (Figures 4F and 4J) and the size of the NBs
280 was much larger (Figure 4N). The increased diameter was not simply due to overexpression of
281 two folds of TDP-43 protein, as co-expression of WT TDP-43-HA and WT Myc-TDP-43 did not
282 manifest such effect (Figures 4E, 4I, and 4M). Consistent with our hypothesis, ΔRRM2
283 co-expressed with WT TDP-43 was mainly located in the core of the stress-induced NBs
284 (Figures 4G and 4K), and the size was significantly smaller than WT TDP-43 NBs (Figure 4O).

285 The core-shell organization could also be clearly seen when ΔRRM1 and ΔRRM2 TDP-43 were
286 co-expressed (Figures 4H, 4L, and 4P).
287 Next, we characterized the co-localization profiles of the above TDP-43 nuclear structures
288 with paraspeckles by co-immunostaining of NONO and super-resolution microscopy. Of note,
289 NONO is a paraspeckle protein known to reside in the core of paraspeckles (West et al., 2016).
290 Consistently, NONO also showed up in the core of WT TDP-43 NBs (Figure 4Q), which was
291 more obvious when overlaid with ΔRRM2 (Figure 4S). Interestingly, although the ring-shaped
292 structure of ΔRRM1 co-localized and surrounded WT TDP-43 NBs (Figures 4F and 4J), it no
293 longer co-localized with paraspeckles labeled by NONO (Figure 4R). These results indicate that
294 TDP-43 requires the RRM1 domain to be associated with paraspeckles. Also, they confirm that
295 TDP-43 NBs are not homogenous, although a significant subpopulation overlapped with
296 paraspeckles (Figures S1). Together, these data suggest that RRM1 and RRM2 play distinct
297 functions in the assembly and maintenance of TDP-43 NBs, possibly by interacting with different
298 RNAs and/or different RBPs.
299
300 **RNA suppresses TDP-43 *in vitro* de-mixing via the RRMs**
301 The dynamic, reversible and membraneless characteristics of TDP-43 NBs suggested that LLPS
302 might be involved in the formation of TDP-43 NBs. Indeed, purified full-length (FL) TDP-43
303 protein formed LDs *in vitro* in a dose-dependent manner and the LCD played a major role in
304 promoting TDP-43 LLPS (Figures S6A-S6D). Nevertheless, *in vitro* de-mixing of the C-terminal
305 LCD truncation (TDP-43^{1-274}) was evident at a higher protein concentration (≥50 μM) (Figure
306 S6D), which was consistent with the previous report that the N-terminal domains of TDP-43
307 could drive LLPS *in vivo* (Schmidt and Rohatgi, 2016). Next, we examined how RNA impacted
308 on TDP-43 LLPS by adding total RNAs extracted from HeLa cells into the *in vitro* de-mixing
309 system (Figures S6E and S6F). Total RNAs (500 ng/μl) markedly reduced the LLPS of FL
310 TDP-43 (Figure S6E), whereas much lower concentrations of total RNAs (≥100 ng/μl) were
311 sufficient to suppress the LLPS of TDP-43^{1-274} (Figure S6F). Of note, the presence of the LCD

312 made the purified FL TDP-43 protein extremely insoluble, for which a sumo tag was needed all
313 the time to keep FL TDP-43 protein from precipitation *in vitro*. However, the solubilizing sumo tag
314 made it difficult to assess and compare the role of the two RRMs in mediating RNA suppression,
315 as large SUMO-TDP-43 droplets were tricky to form or maintain (Figures S6G-S6I). Thus, we
316 used the TDP-43$^{1-274}$ protein (which did not require the sumo tag to stay soluble) in the
317 subsequent experiments (Figures S6J-S6L and Figure 5). In addition, we confirmed that the
318 RNA-binding affinity was significantly reduced in ΔRRM1 and ΔRRM2 TDP-43$^{1-274}$ (Figures
319 S6M-S6O).

320 Both WT TDP-43$^{1-274}$ and the two RRM mutants formed LDs in a dose-dependent manner in
321 the *in vitro* LLPS system, though the de-mixing of ΔRRM1 TDP-43$^{1-274}$ was less robust (Figures
322 S6J-S6L). To facilitate the subsequent evaluation, we lowered the NaCl concentration and
323 increased the crowding agent PEG, which allowed larger TDP-43 LDs to form at the beginning of
324 the suppression assay (Figures 5B-5D). We found that total RNAs at a concentration of 100 ng/μl
325 markedly reduced the size and number of WT TDP-43$^{1-274}$ LDs. ΔRRM1 TDP-43$^{1-274}$ (50 μM) only
326 formed small LDs, which initially made us presume the LLPS of ΔRRM1 would be more easily
327 suppressed by total RNAs. To our surprise, a much higher concentration of total RNAs (≥500
328 ng/μl) was required (Figure 5C). We also tested ΔRRM1 at a higher concentration (100 μM) to
329 allow large ΔRRM1 LDs to form at the beginning, and the results confirmed the drastically
330 reduced RNA suppression of the LLPS of ΔRRM1 TDP-43$^{1-274}$ (total RNAs ≥250 ng/μl) (Figure
331 5C'). The RNA suppression of the LLPS of ΔRRM2 TDP-43$^{1-274}$ was also reduced, but to a less
332 extent than that of ΔRRM1 (100~250 ng/μl total RNAs) (Figures 5B-5D). It was worth noting that
333 ΔRRM1 TDP-43$^{1-274}$ showed both decreased LLPS capacity and reduced sensitivity to RNA
334 suppression, indicating that a RBP with lower tendency to phase separate does not necessarily
335 mean that RNA would more potently suppress its LLPS. Rather, the regulation by RNAs is likely
336 to be specific and different depending on the type and structure of the RNAs.

337 tRNA reduced the LLPS of FUS *in vitro* (Maharana et al., 2018), which also potently
338 suppressed the *in vitro* de-mixing of TDP-43 (Figure 5E). Further, we found that WT and ΔRRM1

339 TDP-43$^{1-274}$ showed similar sensitivity to tRNA (≥1.25 μg/μl) (Figures 5E and 5F), whereas
340 ΔRRM2 required a higher concentration of tRNA (≥2.5 μg/μl) to reach the similar extent of
341 suppression (Figure 5G). It should be pointed out that, unlike the response to total RNAs,
342 ΔRRM1 TDP-43$^{1-274}$ did not exhibit a greatly decreased sensitivity to tRNA suppression (Figures
343 5C and 5F). Thus, the lack of a strong suppression of the LLPS of ΔRRM1 by total RNAs was not
344 simply because suppression of small LDs was difficult to manifest or detect. Taken together,
345 RRM1 appeared to play a major role in mediating total RNA suppression of TDP-43 LLPS
346 (Figures 5B-5D), whereas RRM2 might be specifically involved in the suppression by certain
347 RNAs such as tRNA (Figures 5E-5G).
348

349 **Paraspeckle RNA *NEAT1* promotes TDP-43 LLPS and is upregulated in stressed neurons**

350 Recent works have revealed both positive and negative regulation of LLPS of prion-like RBPs by
351 RNAs (Guo and Shorter, 2015). Since stress-induced TDP-43 NBs were partially co-localized
352 with paraspeckles (Figures S1A and S1B), we examined whether the paraspeckle scaffolding
353 RNA *NEAT1* impacted on the phase behavior of TDP-43. We showed that *NEAT1* RNA could
354 directly bind to TDP-43 protein in the *in vitro* dot-blot assay (Figure 5H). Further, addition of
355 *NEAT1* RNA into the *in vitro* de-mixing system promoted TDP-43 LLPS in a dose-dependent
356 manner (Figure 5I), and this effect involved both RRM1 and RRM2 (Figures 5J and 5K).
357 Furthermore, we revealed that increasing concentrations of *NEAT1* antagonized the suppressive
358 environment generated by tRNA in the *in vitro* LLPS assay (Figure 5L). Moreover, the promotion
359 of TDP-43 LLPS by *NEAT1* was markedly reduced in ΔRRM1 but enhanced in ΔRRM2 (Figures
360 5M and 5N), suggesting that, in a complex system containing both positive and negative
361 regulatory RNAs, such as in the nucleoplasm, the RRM1 of TDP-43 may play a major role in
362 mediating the *NEAT1*-promotion of TDP-43 LLPS whereas the RRM2 may be more involved in
363 the tRNA-mediated suppression.

364 Furthermore, we examined the RNA-binding affinity of the NES^{mut} and found that it was
365 significantly lower than that of WT TDP-43 (Figures S3G-S3H), which confirmed the previous

366 reports that the NES^{mut} impaired RNA binding of TDP-43 (Lukavsky et al., 2013; Flores et al.,
367 2019). Consistently, the K145/192Q mutation also showed reduced RNA binding (Figures
368 S3E-S3F), and the suppression of TDP-43 LLPS by total RNAs was decreased with the
369 K145/192Q (Figures S3I-S3J). Interestingly, the K145/192R mutation did not appear to improve
370 RNA binding (Figure S3E-S3H) or enhance the suppression of TDP-43 LLPS by total RNAs
371 (Figure S3K). Instead, it disrupted *NEAT1*-mediated nucleation of TDP-43 droplets (Figures
372 S3L-S3N), which might "complement" the lack of RNA suppression in the NES^{mut} and thus
373 reversed the spontaneous NB formation in TDP-43-NES^{mut}-K145/192R (Figures 3F-3F' and 3H)
374 and regained cytotoxicity (Figure 3L). These data suggest a vital role of *NEAT1* in the formation
375 of TDP-43 NBs.

376 Next, we extended our investigation of TDP-43 NBs and *NEAT1* to mammalian neurons. We
377 confirmed that TDP-43 formed NBs in mouse primary neurons in response to stress (Figures
378 5O-5O', 5R and 5U). Consistent with the phenotypes in HeLa and 293T cells, ΔRRM1 showed
379 large ring-shaped structures in both non-stressed and stressed mouse neurons (Figures 5P-5P'
380 and 5S), whereas ΔRRM2 displayed a grainy appearance when neurons were treated with
381 arsenite (Figures 5Q-5Q' and 5T). More importantly, we found that the levels of both total *NEAT1*
382 RNA and the lncRNA isoform *NEAT1_2* were dramatically increased in mouse primary neurons
383 treated with arsenite (Figure 5V) as well as LMB (Figure 5W). Together with the *in vitro* LLPS
384 data (Figures 5L-5N), these data suggest that stress may trigger an upregulation of *NEAT1* RNA,
385 which provides nucleation scaffolds to condense TDP-43 and possibly other NB components by
386 promoting the LLPS, thereby antagonizing the suppressive environment of the nucleoplasm and
387 causing the formation of TDP-43 NBs.

388

389 **ALS-associated D169G mutation of TDP-43 shows a specific defect in NB formation**

390 This study was launched by the discovery that TDP-43 formed dynamic and reversible NBs in
391 stressed cells and the formation of NBs alleviated TDP-43-mediated cytotoxicity. To further
392 investigate the disease relevance of TDP-43 NBs, we examined several known ALS-causing

393 mutations in TDP-43. Interestingly, we found that the mutation of D169G (640A→T) within the
394 RRM1 (Kabashi et al., 2008; and Figures 6A-6B) drastically reduced the assembly of TDP-43
395 NBs induced by either arsenite (250 μM, 30 min) (Figures 6C-6E) or LMB (25 nM, 12 h) (Figures
396 S7A-S7C). In contrast, the assembly of SGs or the recruitment of TDP-43-D169G to SGs was
397 not diminished at this condition (Figures 6C and 6F). Unlike D169G, the disease-associated
398 mutations in the LCD region such as Q331K and M337V did not hindered the stress-induced
399 assembly of TDP-43 NBs (Figures S7D-S7G). Thus, the D169G mutation specifically impaired
400 the assembly of stress-induced TDP-43 NBs. In addition, the difference between D169G and
401 other disease mutations enriched in the LCD also suggests that although TDP-43 NBs and SGs
402 are both phase-separated, membraneless RNP granules, the exact mechanisms regulating their
403 formation can be different.

404 Next, we increased the duration of arsenite treatment (250 μM, 120 min) to test if D169G
405 could eventually form TDP-43 NBs with prolonged stress, which indeed occurred (Figures
406 6C-6E). However, what was unexpected and surprised us was that there were staggeringly more
407 cells forming TDP-43^{+} SGs in D169G (75.6% ± 3.8%) than WT TDP-43 (31.3 ± 2.3%) with
408 prolonged stress (Figures 6C and 6F). It has been proposed that TDP-43 recruited to SGs
409 becomes phosphorylated, which promotes aberrant phase transition of SGs to cytoplasmic
410 protein inclusions (Li et al., 2013). And, phosphorylation of TDP-43 (pTDP-43) at S409/410
411 (pS409/410) is a disease-specific marker of TDP-43 aggregates (Hasegawa et al., 2008;
412 Neumann et al., 2009). Immunostaining for pS409/410 revealed that the NB-forming defective
413 D169G formed pTDP-43 cytoplasmic foci in prolonged stress (arsenite 250 μM, 6 h), which was
414 not observed in WT TDP-43 under the same condition (Figures 6G-6I). Of note, like WT TDP-43
415 (Figure 6G), D169G in the nucleus was absent of pS409/410 staining even with prolonged stress
416 (Figure 6H), indicating that TDP-43-D169G was not generally hyperphosphorylated but rather
417 only when it formed abnormal cytoplasmic foci. Moreover, cells expressing D169G showed
418 significantly more death during prolonged stress (arsenite 100 μM, 12 h) than cells expressing
419 WT TDP-43 (Figures 6J-6K). These results suggest that the assembly of TDP-43 NBs acts as an

420 important stress response mechanism, which may lower the demand for the formation of SGs
421 and prevent excessive cytoplasmic translocation of TDP-43, therefore reducing the chance of
422 aberrant phase transition and the accumulation of pathogenic pTDP-43 inclusions in the
423 cytoplasm.

424 To further assess the cytotoxicity of the D169G mutation in an *in vivo* setting, we generated
425 transgenic flies expressing *hTDP-43-D169G* (Figure 6L-6M). These flies exhibited
426 age-dependent degeneration of the eyes (Figure 6N), and the enhanced neurotoxicity was more
427 evident when the D169G mutant was expressed in fly motor neurons – the climbing capability
428 showed an accelerated decline compared to the flies expressing *WT-hTDP-43*, especially at later
429 time points in aged flies (Figure 6O, Day 21 and Day 27). As aging is associated with cumulative
430 stress and is a risk factor for neurodegenerative diseases (Lopez-Otin et al., 2013; Hou et al.,
431 2019), these results further support the idea that the D169G mutation makes cells more prone to
432 stress, which may underlie its pathogenesis in the ALS disease.

433

434 **The D169G mutation diminishes lncRNA *NEAT1*-mediated TDP-43 LLPS *in vitro* and NB**
435 **formation in cells**

436 To understand the molecular basis for the NB-forming deficit of D169G, we then examined the
437 phase separation behavior of TDP-43-D169G. The results of the *in vitro* LLPS assay showed that
438 D169G TDP-43^{1-274} protein formed LDs in a dose-dependent manner just like that of WT (Figures
439 7A-7B), which indicated that the ability of D169G to phase separate was not markedly changed.
440 The dot-blot assay confirmed the previous report (Kuo et al., 2014) the binding affinity of D169G
441 to total RNAs was not reduced compared to that of WT TDP-43 (Figures S7H-S7J). And,
442 suppression of TDP-43 LLPS by total RNA extracts showed no marked difference in D169G
443 compared to that of WT TDP-43^{1-274} (Figures 7C and 7D). Thus, the general regulation of
444 TDP-43 RNP granules by total RNAs remained largely intact in D169G, which was consistent
445 with the fact that D169G did not hinder SG formation in stressed cells (Figures 6C and 6F).

446 In striking contrast, the induction of TDP-43 LLPS by *NEAT1* RNA was drastically reduced in
447 D169G (Figures 7E and 7F). We then performed the RNA electrophoretic mobility shift assay
448 (EMSA) to evaluate and compare the RNA binding affinity of WT and D169G TDP-43. Incubation
449 of the TDP-43 proteins with *NEAT1* RNA markedly slowed down the migration speed of the latter,
450 which led to a dosage-dependent band shift (Figure 7G). The impact on band shifts caused by
451 D169G was significantly smaller than that of WT TDP-43 (Figures 7G-7H), indicating that the
452 binding affinity of D169G to *NEAT1* is reduced. However, we did notice that at a higher protein
453 concentration (16 μM), the difference between D169G and WT TDP-43 became smaller. This
454 again points tothat the concentrations of nuclear RNAs and proteins are crucial for the
455 assembly-disassembly of TDP-43 NBs, which may partially explain why the stress-induced NB
456 formation of D169G is delayed but not completely abolished (Figures 6C-6E).

457 To confirm the above *in vitro* findings in the intracellular milieu of mammalian cells, we
458 conducted fluorescence in situ hybridization (FISH) for *NEAT1* lncRNA together with fluorescent
459 immunocytochemistry for WT and D169G TDP-43 in human HeLa cells. We found that stress
460 significantly increased the colocalization of *NEAT1* FISH-RNA foci with WT TDP-43 NBs
461 (Figures 7I-7J, 7M-7N). In contrast, an increase of the colocalization of *NEAT1* lncRNA foci with
462 TDP-43 NBs by stress was not observed with D169G TDP-43 (Figures 7K-7L, 7O-7P),
463 suggesting that *NEAT1* was unable to promote the assembly of D169G TDP-43 NBs in cells *in*
464 *vivo*. To further confirm the requirement of lncRNA *NEAT1* in the assembly of TDP-43 NBs, we
465 knocked down *NEAT1* by small interfering RNA (siRNA) (Figures 7Q and 7R). Under this
466 condition, the numbers of stress-induced *NEAT1* puncta and TDP-43 NBs are both dramatically
467 reduced (Figures 7S-7W). Together, our findings propose that the paraspeckle scaffolding
468 lncRNA *NEAT1* mediates the assembly of TDP-43 NBs, which may be an important mechanism
469 to mitigate stress and alleviate cytotoxicity, and a compromise of the TDP-43 NB-mediated
470 stress-mitigating mechanism may lead to excessive cytoplasmic translocation and accumulation
471 of ALS-pathogenic, phosphorylated TDP-43 protein inclusions.
472

473 **DISCUSSION**

474 **The stress-induced TDP-43 NB and its cytotoxicity-antagonizing role**

475 This study was initiated by the observation of distinct TDP-43 nuclear granules in stressed cells.
476 We then characterized these subnuclear structures and demonstrated that they meet the three
477 criteria of NBs (Stanek and Fox, 2017) – (1) microscopically distinctive; (2) enriched of TDP-43
478 and partially colocalized with paraspeckles; and (3) highly dynamic and sensitive to the
479 surrounding nucleoplasm. Various cellular stresses such as arsenic stress, nuclear export
480 blockage, and proteasomal inhibition trigger the formation of TDP-43 NBs. And, TDP-43 NBs are
481 observed in stressed human cells, mouse primary neurons, and *Drosophila* brains *in vivo*. In
482 addition, a recent paper by Gasset-Rosa et al. (2019) showed that TDP-43 at its endogenous
483 level forms nuclear droplets in multiple cell types. Thus, the assembly of TDP-43 NBs occurs in
484 multiple cell types and in different organisms, suggesting a general role and wide participation of
485 TDP-43 NBs in response to cellular stress.

486 We show in this study that NB-forming TDP-43 such as the NES^{mut} and the K145/192Q
487 mutation are much less cytotoxic than diffused WT TDP-43. More importantly, abolishing the
488 capability of TDP-43-NES^{mut} to form NBs makes the originally non-toxic NES^{mut} exhibit
489 cytotoxicity. How do TDP-43 NBs acquire cytoprotection? It is thought that SGs help cells survive
490 stress by sequestering mRNAs and temporarily arresting protein synthesis (Liu-Yesucevitz et al.,
491 2010). Given that TDP-43 plays an important role in regulating gene expression and RNA
492 metabolism (Tollervey et al., 2010; Han et al., 2012; Seo et al., 2016) and is presented in both
493 SGs and TDP-43 NBs, it is reasonable to speculate that a similar underpinning mechanism may
494 contribute to the cytoprotective function of TDP-43 NBs. For example, the assembly of TDP-43
495 NBs may stall DNA transcription and/or arrest RNA processing in stressed cells; when stress is
496 relieved, TDP-43 NBs disassemble and release the RNAs and nuclear proteins required for
497 normal cell functions. In addition, our data indicate that TDP-43 NBs can become irreversible
498 protein aggregates under prolonged stress, which is consistent with the observation of
499 intranuclear inclusions of TDP-43 in some ALS cases (Forman et al., 2007).

500

501 **The organization of TDP-43 NBs and the functions of the two RRMs**

502 Super-resolution microscopy imaging reveals a core-shell organization of TDP-43 NBs,
503 regulated by the two RRMs differently. TDP-43 contains two canonical RRMs in tandem. RRM1
504 has a longer Loop3 region than RRM2 and is thought to have a higher affinity for RNA targets
505 (Buratti and Barall, 2001; Kuo et al., 2014). Although ΔRRM1 and ΔRRM2 show similar binding
506 affinity to total RNAs in the dot-blot assay, they do display divergent sensitivities to RNA
507 suppression in the *in vitro* LLPS assays. For example, suppression of TDP-43 LLPS by total
508 RNAs is greatly reduced in ΔRRM1 but only slightly decreased in ΔRRM2. Another example is
509 the assay using tRNA to mimic nucleoplasmic suppression, in which the induction of TDP-43
510 LLPS by *NEAT1* RNA is much reduced in ΔRRM1 but increased in ΔRRM2.

511 In cells, WT TDP-43 is diffused in the nucleus under normal conditions and phase separate
512 into NBs when cells are stressed. ΔRRM1 lacks the RRM1-dependent total RNA suppression,
513 leading to spontaneous partition of ΔRRM1 into phase-separated intranuclear droplets.
514 Meanwhile, TDP-43 likely interacts with nucleation factors such as *NEAT1* RNA via the RRM1,
515 which anchors TDP-43 to the core of NBs. As such, without the "centripetal force",
516 TDP-43-ΔRRM1 is mainly presented in the shell and forms large, ring-shaped subnuclear
517 structures, and stress does not further promote ΔRRM1 to form normal NBs or additional
518 ring-shaped structures. Thus, the RRM1 appears to execute the seemingly conflicting functions –
519 suppressing TDP-43 phase separation under normal conditions whereas condensing TDP-43 to
520 the core of NBs when the LLPS occurs, which might be attained by interacting with different
521 RNAs. In contrast, since ΔRRM2 retains the main RNA suppression mediated by the RRM1, it
522 does not spontaneously phase separate like ΔRRM1. When cells are stressed and the
523 intracellular LLPS of TDP-43 is initiated, ΔRRM2 that lacks the "centrifugal force" to counteract
524 the RRM1-mediated "centripetal force" is condensed to the core and forms small, insoluble NBs.
525 We speculate that the distinct roles of the two RRMs in regulating the assembly of TDP-43 NBs
526 may result from different RNA-recognition patterns and binding preferences. This idea is

527 supported by the later observations in this study that the RRM1 and the RRM2 mediate the
528 promotion of TDP-43 LLPS by *NEAT1* lncRNA and the suppression by tRNA, respectively.
529 Together, we propose a "push-and-pull" model for the distinct functions of the two RRMs in
530 maintaining the "core-shell" organization of TDP-43 NBs.
531

532 **The role of lncRNA *NEAT1* in the assembly of TDP-43 NBs**

533 LncRNAs are thought to provide the scaffold for the assembly of NBs such as paraspeckles
534 (Clemson et al., 2009; Chen and Carmichael, 2009; Yamazaki et al., 2018) and nuclear stress
535 bodies (Jolly et al., 2004; Valgardsdottir et al., 2005). In particular, the paraspeckle lncRNA
536 *NEAT1* are increased in patients and/or animal models of several neurodegenerative diseases
537 including ALS (Nishimoto et al., 2013), Alzheimer's disease (Puthlyedth et al., 2016), Parkinson's
538 disease (Mariani et al., 2016), Huntington's disease (Cheng et al., 2018), and multiple sclerosis
539 (Schirmer et al., 2019).

540 In this study, we find that *NEAT1* lncRNA is substantially upregulated in stressed neurons
541 and TDP-43 NBs are partially colocalized with *NEAT1* lncRNA foci. In the meanwhile,
542 knockdown of *NEAT1* substantially reduces the formation of stress-induced TDP-43 NBs.
543 Further *in vitro* experiments indicate that *NEAT1* not only promotes TDP-43 LLPS, but also
544 antagonizes the "suppressive" environment modeled with tRNA. As *NEAT1_2* is a lncRNA over
545 20 kb in length and has complex secondary structures, we speculate that it may provide multiple
546 binding sites for gathering TDP-43 molecules (and potentially other *NEAT1*-binding proteins)
547 together. This would increase the multivalent interactions leading to co-phase separation of
548 TDP-43 and *NEAT1*. In contrast, shorter RNAs such as tRNA lacking long stretches to
549 accommodate multiple TDP-43 molecules may instead segregate each individual TDP-43,
550 therefore suppressing the phase separation. As such, stress-induced upregulation of *NEAT1*
551 may provide nucleation scaffolds to concentrate TDP-43 and other NB proteins, overturning the
552 suppressive environment in the nucleoplasm, leading to the emergence of TDP-43 NBs. It is
553 worth noting that lncRNAs such as *NEAT1* are RNA targets of TDP-43 (Polymenidou et al., 2011;

554 Chung et al., 2018; Modic et al., 2019), implying that complicated cross-regulations between
555 TDP-43 and *NEAT1* as well as between SGs and paraspeckles (An et al. 2019) might be
556 involved in stress and diseases.
557

558 **The D169G mutation and the relevance of TDP-43 NBs in ALS pathogenesis**

559 More than 30 disease-causing mutations have been identified in TDP-43, most of which are in
560 the LCD and the adjacent regions (Chen-Plotkin et al., 2010; Lee et al., 2011). D169G is the only
561 known ALS-causing mutation within the RRM1 of TDP-43 (Kabashi et al., 2008) and its
562 pathogenic mechanism has been elusive. Initially, it was presumed to abrogate RNA binding due
563 to its location within the RRM (Kabashi et al., 2008). However, subsequent work indicates that
564 the mutation by D169G causes a small local conformational change in the Turn6 of the β-sheets
565 within the RRM1 of TDP-43 (Austin et al., 2014; Chiang et al., 2016), but does not reduce the
566 overall binding affinity of TDP-43 to RNA or DNA (Kuo et al., 2014). And, although D169G
567 exhibits slightly increased thermal stability and may be more susceptible to proteolytic cleavage
568 (Austin et al., 2014; Chiang et al., 2016), it does not engender aberrant oligomerization but rather
569 increases the resistance of TDP-43 to aggregation (Austin et al., 2014). The only known major
570 cellular alteration by D169G is that it reduces polyubiquitination and the co-aggregation of
571 TDP-43 with Ubiquilin 1 (Kim et al., 2009). However, given the long-standing notion that
572 cytoplasmic inclusions containing ubiquitinated TDP-43 is a pathological hallmark and cause of
573 the disease (Li et al., 2013; Jovičić et al., 2016; Zhao et al., 2018), it has been difficult to
574 understand how decreased ubiquitination and aggregation of TDP-43-D169G causes ALS.

575 In this study, we discover that D169G has a striking and specific deficit in stress-induced
576 TDP-43 NBs. In line with that, the induction of TDP-43 LLPS by *NEAT1* is dramatically
577 diminished in the *in vitro* assay and the co-localization of TDP-43 NBs with *NEAT1* lncRNA foci is
578 also reduced in D169G. In contrast, the suppression of TDP-43 LLPS by total RNAs is
579 unaffected by D169G and the recruitment of D169G to SGs is not impeded. Instead, the
580 NB-forming defective D169G forms significantly more TDP-43^{+} SGs when cells are subjected to

581 prolonged cellular stress, which gives rise to cytoplasmic TDP-43 foci that are marked with the
582 phosphorylation disease hallmark pS409/410. Together, we propose that the stress-induced
583 upregulation of lncRNA *NEAT1* promotes the assembly of TDP-43 NBs via LLPS, which may be
584 called up to engage in the first line of defense against cellular stresses and disease conditions.
585 Prompt assembly of TDP-43 NBs may lower the need for forming cytoplasmic SGs and prevents
586 excessive cytoplasmic translocation and accumulation of TDP-43. The ALS-causing D169G
587 mutation provides a paradigm for compromise of TDP-43 NBs leading to abnormal cytoplasmic
588 foci containing pTDP-43, which may contribute to ALS pathogenesis. Given that cytoplasmic
589 mislocalization and nuclear depletion of TDP-43 are common in diseased neurons, it is likely that
590 loss of the TDP-43 NB-mediated stress-mitigating function may also underlie other cases of ALS
591 and related diseases.

ACKNOWLEDGMENTS

We thank the BDSC for providing the fly strains, the SIBCB *Drosophila* Center for the fly embryo injection services, L. Chen, L. Pan, J. Zhou, and Z. Zhang for the cloning vectors and plasmids, Z. Zhang for help in the pulse-chase assay, S. Qiu for technical supports, J. Yuan, A. Li, Y. Chen and Z. He for comments and critical reading of the manuscript, and the members of the Fang lab for helpful discussion. **Funding**: Supported by grants from the National Key R&D Program of China (No. 2016YFA0501902) to Y.F. and C.L., the National Natural Science Foundation of China (No. 81671254 and No. 31471017) to Y.F and (No. 91853112 and No. 31470748) to C.L, the Shanghai Municipal Science and Technology Major Project (No. 2019SHZDZX02) to Y.F and C.L, the Science and Technology Commission of Shanghai Municipality (18JC1420500) to C.L, and the Alzheimer's Association (AARF-16-441196) and Target ALS Springboard Fellowship to L.G. **Author contributions:** G.D., Z.M. and Y.F. conceived the research; C.W., Y.D., G.D., C.L., L.G. and Y.F. designed the experiments; C.W., Y.D. G.D., Q.W., K.Z., X.D., B.Q., J.G. and S.Z. performed the experiments; C.W., Y.D., G.D., Q.W., Z.M., J.G. and C.L contributed important new reagents; C.W., Y.D. G.D., and Y.F. analyzed the data and interpreted the results; C.W., Y.D., G.D. and Y.F. prepared the figures; and C.W., Y.D. G.D., C.L. and Y.F. wrote the paper. All authors read and approved the final manuscript. **Competing interests:** None. **Data and materials availability:** All data are available in the manuscript or the supplementary materials.

SUPPLEMENTAL INFORMATION

Online Methods

Figures S1-S7

Videos S1-S2

615 **REFERENCES**

616 Austin, J.A., Wright, G.S., Watanabe, S., Grossmann, J.G., Antonyuk, S.V., Yamanaka, K. and
617 Hasnain, S.S. (2014) Disease causing mutants of TDP-43 nucleic acid binding domains are
618 resistant to aggregation and have increased stability and half-life. *Proc Natl Acad Sci U S A*,
619 **111**, 4309-4314.

620 An, H., Skelt, L., Notaro, A., Highley, J.R., Fox, A.H., La Bella, V., Buchman, V.L. and
621 Shelkovnikova, T.A. (2019) ALS-linked FUS mutations confer loss and gain of function in the
622 nucleus by promoting excessive formation of dysfunctional paraspeckles. *Acta Neuropathol*
623 *Commun,* **7**, 7.

624 An, H., Tan, J.T., and Shelkovnikova, T.A. (2019). Stress granules regulate stress-induced
625 paraspeckle assembly. *J Cell Biol. [Epub ahead of print]*

626 Banani, S.F., Lee, H.O., Hyman, A.A. and Rosen, M.K. (2017) Biomolecular condensates:
627 organizers of cellular biochemistry. *Nat Rev Mol Cell Biol,* **18**, 285-298.

628 Barmada, S.J., Skibinski, G., Korb, E., Rao, E.J., Wu, J.Y., and Finkbeiner, S. (2010)
629 Cytoplasmic mislocalization of TDP-43 is toxic to neurons and enhanced by a mutation
630 associated with familial amyotrophic lateral sclerosis. *J Neurosci*, **30**, 639-649.

631 Bateman, J.R., Lee, A.M., and Wu, C.T. (2006). Site-specific transformation of Drosophila via
632 phiC31 integrase-mediated cassette exchange. *Genetics*, **173**, 769-777.

633 Bernstam, L. and Nriagu, J. (2000) Molecular aspects of arsenic stress. *J Toxicol Environ Health*
634 *B Crit Rev,* **3**, 293-322.

635 Bond, C.S., and Fox, A.H. (2009). Paraspeckles: nuclear bodies built on long noncoding RNA. J
636 Cell Biol 186, 637-644.

637 Brady, O.A., Meng, P., Zheng, Y., Mao, Y. and Hu, F. (2011) Regulation of TDP-43 aggregation
638 by phosphorylation and p62/SQSTM1. *J Neurochem,* **116**, 248-259.

639 Buratti, E. and Baralle, F.E. (2001) Characterization and functional implications of the RNA
640 binding properties of nuclear factor TDP-43, a novel splicing regulator of CFTR exon 9. *J*
641 *Biol Chem,* **276**, 36337-36343.

642 Burke, K.A., Janke, A.M., Rhine, C.L. and Fawzi, N.L. (2015) Residue-by-Residue View of In
643 Vitro FUS Granules that Bind the C-Terminal Domain of RNA Polymerase II. *Mol Cell,* **60**,
644 231-241.

645 Cao, X., Wang, H., Wang, Z., Wang, Q., Zhang, S., Deng, Y. and Fang, Y. (2017) In vivo imaging
646 reveals mitophagy independence in the maintenance of axonal mitochondria during normal
647 aging. *Aging Cell*, **16**, 1180-1190.

648 Chen, L.L. and Carmichael, G.G. (2009) Altered nuclear retention of mRNAs containing inverted
649 repeats in human embryonic stem cells: functional role of a nuclear noncoding RNA. *Mol*

650 *Cell,* **35**, 467-478.

651 Chen-Plotkin, A.S., Lee, V.M., and Trojanowski, J.Q. (2010) TAR DNA-binding protein 43 in
652 neurodegenerative disease. *Nat Rev Neurol*, **6**, 211-220.

653 Cheng, C., Spengler, R.M., Keiser, M.S., Monteys, A.M., Rieders, J.M., Ramachandran, S. and
654 Davidson, B.L. (2018) The long non-coding RNA NEAT1 is elevated in polyglutamine repeat
655 expansion diseases and protects from disease gene-dependent toxicities. *Hum Mol Genet*,
656 **27**, 4303-4314.

657 Chiang, C.H., Grauffel, C., Wu, L.S., Kuo, P.H., Doudeva, L.G., Lim, C., Shen, C.K. and Yuan,
658 H.S. (2016) Structural analysis of disease-related TDP-43 D169G mutation: linking
659 enhanced stability and caspase cleavage efficiency to protein accumulation. *Sci Rep*, **6**,
660 21581.

661 Chung, C.Y., Berson, A., Kennerdell, J.R., Sartoris, A., Unger, T., Porta, S., Kim, H.J., Smith,
662 E.R., Shilatifard, A., Van Deerlin, V., et al. (2018) Aberrant activation of non-coding RNA
663 targets of transcriptional elongation complexes contributes to TDP-43 toxicity. *Nat Commun*,
664 **9**, 4406.

665 Clemson, C.M., Hutchinson, J.N., Sara, S.A., Ensminger, A.W., Fox, A.H., Chess, A. and
666 Lawrence, J.B. (2009) An architectural role for a nuclear noncoding RNA: NEAT1 RNA is
667 essential for the structure of paraspeckles. *Mol Cell,* **33**, 717-726.

668 Cohen, T.J., Hwang, A.W., Restrepo, C.R., Yuan, C.X., Trojanowski, J.Q. and Lee, V.M. (2015)
669 An acetylation switch controls TDP-43 function and aggregation propensity. *Nat Commun,* **6**,
670 5845.

671 Conicella, A.E., Zerze, G.H., Mittal, J., and Fawzi, N.L. (2016). ALS Mutations Disrupt Phase
672 Separation Mediated by alpha-Helical Structure in the TDP-43 Low-Complexity C-Terminal
673 Domain. *Structure* **24**, 1537-1549.

674 Dominguez, D., Freese, P., Alexis, M.S., Su, A., Hochman, M., Palden, T., Bazile, C., Lambert,
675 N.J., Van Nostrand, E.L., Pratt, G.A. et al. (2018) Sequence, Structure, and Context
676 Preferences of Human RNA Binding Proteins. *Mol Cell,* **70**, 854-867 e859.

677 Duan, Y., Du, A., Gu, J., Duan, G., Wang, C., Gui, X., Ma, Z., Qian, B., Deng, X., Zhang, K. et al.
678 (2019) PARylation regulates stress granule dynamics, phase separation, and neurotoxicity
679 of disease-related RNA-binding proteins. *Cell Res,* **29**, 233-247.

680 Ederle, H. and Dormann, D. (2017) TDP-43 and FUS en route from the nucleus to the cytoplasm.
681 *FEBS Letters,* **591**, 1489-1507.

682 Fahrenkrog, B. and Harel, A. (2018) Perturbations in Traffic: Aberrant Nucleocytoplasmic
683 Transport at the Heart of Neurodegeneration. *Cells,* **7**, pii: E232.

684 Feric, M., Vaidya, N., Harmon, T.S., Mitrea, D.M., Zhu, L., Richardson, T.M., Kriwacki, R.W.,
685 Pappu, R.V. and Brangwynne, C.P. (2016) Coexisting Liquid Phases Underlie Nucleolar
686 Subcompartments. *Cell,* **165**, 1686-1697.

687 Flores, B.N., Li, X., Malik, A.M., Martinez, J., Beg, A.A., and Barmada, S.J. (2019) An
688 Intramolecular Salt Bridge Linking TDP43 RNA Binding, Protein Stability, and
689 TDP43-Dependent Neurodegeneration. *Cell Rep*, **27**, 1133-1150.e8.

690 Forman, M.S., Trojanowski, J.Q. and Lee, V.M. (2007) TDP-43: a novel neurodegenerative
691 proteinopathy. *Curr Opin Neurobiol*, **17**, 548-555.

692 Fox, A.H., and Lamond, A.I. (2010). Paraspeckles. Cold Spring Harb Perspect Biol 2, a000687.

693 Fox, A.H., Nakagawa, S., Hirose, T., and Bond, C.S. (2018). Paraspeckles: Where Long
694 Noncoding RNA Meets Phase Separation. Trends Biochem Sci 43, 124-135.

695 Fu, X.D., and Maniatis, T. (1990). Factor required for mammalian spliceosome assembly is
696 localized to discrete regions in the nucleus. Nature 343, 437-441.

697 Gasset-Rosa, F., Lu, S., Yu, H., Chen, C., Melamed, Z., Guo, L., Shorter, J., Da Cruz, S., and
698 Cleveland, D.W. (2019) Cytoplasmic TDP-43 De-mixing Independent of Stress Granules
699 Drives Inhibition of Nuclear Import, Loss of Nuclear TDP-43, and Cell Death. *Neuron*, **102**,
700 339-357.e7.

701 Groth, A.C., Fish, M., Nusse, R., and Calos, M.P. (2003). Construction of transgenic Drosophila
702 by using the site-specific integrase from phage PhiC31. *Genetics*, **166**, 1775-1782.

703 Guo, L. and Shorter, J. (2015) It's Raining Liquids: RNA Tunes Viscoelasticity and Dynamics of
704 Membraneless Organelles. *Mol Cell,* **60**, 189-192.

705 Hasegawa, M., Arai, T., Nonaka, T., Kametani, F., Yoshida, M., Hashizume, Y., Beach, T.G.,
706 Buratti, E., Baralle, F., Morita, M., et al. (2008). Phosphorylated TDP-43 in frontotemporal
707 lobar degeneration and amyotrophic lateral sclerosis. Ann Neurol 64, 60-70.

708 Hennig, S., Kong, G., Mannen, T., Sadowska, A., Kobelke, S., Blythe, A., Knott, G.J., Iyer, K.S.,
709 Ho, D., Newcombe, E.A. et al. (2015) Prion-like domains in RNA binding proteins are
710 essential for building subnuclear paraspeckles. *J Cell Biol,* **210**, 529-539.

711 Hirose, T., Virnicchi, G., Tanigawa, A., Naganuma, T., Li, R., Kimura, H., Yokoi, T., Nakagawa,
712 S., Benard, M., Fox, A.H. et al. (2014) NEAT1 long noncoding RNA regulates transcription
713 via protein sequestration within subnuclear bodies. *Mol Biol Cell*, **25**, 169-183.

714 Hofweber, M., Hutten, S., Bourgeois, B., Spreitzer, E., Niedner-Boblenz, A., Schifferer, M.,
715 Ruepp, M.D., Simons, M., Niessing, D., Madl, T. et al. (2018) Phase Separation of FUS Is
716 Suppressed by Its Nuclear Import Receptor and Arginine Methylation. *Cell,* **173**, 706-719
717 e713.

718 Hou, Y., Dan, X., Babbar, M., Wei, Y., Hasselbalch, S.G., Croteau, D.L., and Bohr, V.A. (2019)
719 Ageing as a risk factor for neurodegenerative disease. *Nat Rev Neurol*, **15**, 565-581.

720 Hyman, A.A., Weber, C.A. and Julicher, F. (2014) Liquid-liquid phase separation in biology. *Annu*
721 *Rev Cell Dev Biol,* **30**, 39-58.

722 Ishihara, T., Ariizumi, Y., Shiga, A., Kato, T., Tan, C.F., Sato, T., Miki, Y., Yokoo, M., Fujino, T.,

723 Koyama, A. et al. (2013) Decreased number of Gemini of coiled bodies and U12 snRNA
724 level in amyotrophic lateral sclerosis. *Hum Mol Genet,* **22**, 4136-4147.

725 Jolly, C., Metz, A., Govin, J., Vigneron, M., Turner, B.M., Khochbin, S. and Vourc'h, C. (2004)
726 Stress-induced transcription of satellite III repeats. *J Cell Biol,* **164**, 25-33.

727 Jovičić, A., Paul, J.W., 3rd and Gitler, A.D. (2016) Nuclear transport dysfunction: a common
728 theme in amyotrophic lateral sclerosis and frontotemporal dementia. *J Neurochem,* **138**
729 **Suppl 1**, 134-144.

730 Kabashi, E., Valdmanis, P.N., Dion, P., Spiegelman, D., McConkey, B.J., Vande Velde, C.,
731 Bouchard, J.P., Lacomblez, L., Pochigaeva, K., Salachas, F. et al. (2008) TARDBP
732 mutations in individuals with sporadic and familial amyotrophic lateral sclerosis. *Nat Genet,*
733 **40**, 572-574.

734 Kim, S.H., Shi, Y., Hanson, K.A., Williams, L.M., Sakasai, R., Bowler, M.J. and Tibbetts, R.S.
735 (2009) Potentiation of amyotrophic lateral sclerosis (ALS)-associated TDP-43 aggregation
736 by the proteasome-targeting factor, ubiquilin 1. *J Biol Chem*, **284**, 8083-8092.

737 Koken, M.H., Puvion-Dutilleul, F., Guillemin, M.C., Viron, A., Linares-Cruz, G., Stuurman, N., de
738 Jong, L., Szostecki, C., Calvo, F., and Chomienne, C. (1994). The t(15;17) translocation
739 alters a nuclear body in a retinoic acid-reversible fashion. The EMBO journal 13, 1073-1083.

740 Kuo, P.H., Chiang, C.H., Wang, Y.T., Doudeva, L.G. and Yuan, H.S. (2014) The crystal structure
741 of TDP-43 RRM1-DNA complex reveals the specific recognition for UG- and TG-rich nucleic
742 acids. *Nucleic Acids Res,* **42**, 4712-4722.

743 Lee, E.B., Lee, V.M., and Trojanowski, J.Q. (2012) Gains or losses: molecular mechanisms of
744 TDP43-mediated neurodegeneration. *Nat Rev Neurosci*, **13**, 38-50.

745 Lee, S., Lee, T.A., Lee, E., Kang, S., Park, A., Kim, S.W., Park, H.J., Yoon, J.H., Ha, S.J., Park, T.
746 et al. (2015) Identification of a subnuclear body involved in sequence-specific cytokine RNA
747 processing. *Nat Commun,* **6**, 5791.

748 Li, W., Reeb, A.N., Lin, B., Subramanian, P., Fey, E.E., Knoverek, C.R., French, R.L., Bigio, E.H.
749 and Ayala, Y.M. (2017) Heat Shock-induced Phosphorylation of TAR DNA-binding Protein
750 43 (TDP-43) by MAPK/ERK Kinase Regulates TDP-43 Function. *J Biol Chem,* **292**,
751 5089-5100.

752 Li, Y.R., King, O.D., Shorter, J. and Gitler, A.D. (2013) Stress granules as crucibles of ALS
753 pathogenesis. *J Cell Biol,* **201**, 361-372.

754 Lin, Y., Protter, D.S., Rosen, M.K. and Parker, R. (2015) Formation and Maturation of
755 Phase-Separated Liquid Droplets by RNA-Binding Proteins. *Mol Cell,* **60**, 208-219.

756 Liu Q and Dreyfuss G. (1996) A novel nuclear structure containing the survival of motor neurons
757 protein. *The EMBO Journal,* **15**, 3555-3565.

758 Liu-Yesucevitz, L., Bilgutay, A., Zhang, Y.J., Vanderweyde, T., Citro, A., Mehta, T., Zaarur, N.,

759 McKee, A., Bowser, R., Sherman, M. et al. (2010) Tar DNA binding protein-43 (TDP-43)
760 associates with stress granules: analysis of cultured cells and pathological brain tissue.
761 *PLoS One*, **5**, e13250.

762 López-Otín, C., Blasco, M.A., Partridge, L., Serrano, M., and Kroemer, G. (2013) The hallmarks
763 of aging. *Cell*, **153**, 1194-1217.

764 Luo, F., Gui, X., Zhou, H., Gu, J., Li, Y., Liu, X., Zhao, M., Li, D., Li, X. and Liu, C. (2018) Atomic
765 structures of FUS LC domain segments reveal bases for reversible amyloid fibril formation.
766 *Nat Struct Mol Biol,* **25**, 341-346.

767 Lukavsky, P.J., Daujotyte, D., Tollervey, J.R., Ule, J., Stuani, C., Buratti, E., Baralle, F.E.,
768 Damberger, F.F., and Allain, F.H. (2013) Molecular basis of UG-rich RNA recognition by the
769 human splicing factor TDP-43. *Nat Struct Mol Biol*, **20**, 1443-1449.

770 Mackenzie, I.R., Nicholson, A.M., Sarkar, M., Messing, J., Purice, M.D., Pottier, C., Annu, K.,
771 Baker, M., Perkerson, R.B., Kurti, A. et al. (2017) TIA1 Mutations in Amyotrophic Lateral
772 Sclerosis and Frontotemporal Dementia Promote Phase Separation and Alter Stress
773 Granule Dynamics. *Neuron,* **95**, 808-816.e809.

774 Maharana, S., Wang, J., Papadopoulos, D.K., Richter, D., Pozniakovsky, A., Poser, I., Bickle, M.,
775 Rizk, S., Guillen-Boixet, J., Franzmann, T.M. et al. (2018) RNA buffers the phase separation
776 behavior of prion-like RNA binding proteins. *Science,* **360**, 918-921.

777 Mann, J.R., Gleixner, A.M., Mauna, J.C., Gomes, E., DeChellis-Marks, M.R., Needham, P.G.,
778 Copley, K.E., Hurtle, B., Portz, B., Pyles, N.J. et al. (2019) RNA Binding Antagonizes
779 Neurotoxic Phase Transitions of TDP-43. *Neuron,* **102***,* 1-18.

780 Mariani, E., Frabetti, F., Tarozzi, A., Pelleri, M.C., Pizzetti, F. and Casadei, R. (2016)
781 Meta-Analysis of Parkinson's Disease Transcriptome Data Using TRAM Software: Whole
782 Substantia Nigra Tissue and Single Dopamine Neuron Differential Gene Expression. *PLoS*
783 *One*, **11**, e0161567.

784 McGurk, L., Gomes, E., Guo, L., Mojsilovic-Petrovic, J., Tran, V., Kalb, R.G., Shorter, J. and
785 Bonini, N.M. (2018) Poly(ADP-Ribose) Prevents Pathological Phase Separation of TDP-43
786 by Promoting Liquid Demixing and Stress Granule Localization. *Molecular Cell,* **71**,
787 703-717.e709.

788 Miguel, L., Frébourg, T., Campion, D., and Lecourtois, M. (2011). Both cytoplasmic and nuclear
789 accumulations of the protein are neurotoxic in Drosophila models of TDP-43 proteinopathies.
790 *Neurobiology of Disease*, **41**, 398-406.

791 Mito, M., Kawaguchi, T., Hirose, T., and Nakagawa, S. (2016). Simultaneous multicolor detection
792 of RNA and proteins using super-resolution microscopy. *Methods*, **98**, 158-165.

793 Modic, M., Grosch, M., Rot, G., Schirge, S., Lepko, T., Yamazaki, T., Lee, F.C.Y., Rusha, E.,
794 Shaposhnikov, D., Palo, M., et al. (2019) Cross-Regulation between TDP-43 and
795 Paraspeckles Promotes Pluripotency-Differentiation Transition. *Mol Cell*, **74**, 951-965 e913.

796 Molliex, A., Temirov, J., Lee, J., Coughlin, M., Kanagaraj, A.P., Kim, H.J., Mittag, T. and Taylor,
797 J.P. (2015) Phase separation by low complexity domains promotes stress granule assembly
798 and drives pathological fibrillization. *Cell,* **163**, 123-133.

799 Murakami, T., Qamar, S., Lin, J.Q., Schierle, G.S., Rees, E., Miyashita, A., Costa, A.R., Dodd,
800 R.B., Chan, F.T., Michel, C.H. et al. (2015) ALS/FTD Mutation-Induced Phase Transition of
801 FUS Liquid Droplets and Reversible Hydrogels into Irreversible Hydrogels Impairs RNP
802 Granule Function. *Neuron,* **88**, 678-690.

803 Murray, D.T., Kato, M., Lin, Y., Thurber, K.R., Hung, I., McKnight, S.L., and Tycko, R. (2017)
804 Structure of FUS Protein Fibrils and Its Relevance to Self-Assembly and Phase Separation
805 of Low-Complexity Domains. *Cell*, **171**, 615-627.

806 Nakagawa, S., Yamazaki, T. and Hirose, T. (2018) Molecular dissection of nuclear paraspeckles:
807 towards understanding the emerging world of the RNP milieu. *Open Biol,* **8,** pii: 180150.

808 Namkoong, S., Ho, A., Woo, Y.M., Kwak, H. and Lee, J.H. (2018) Systematic Characterization of
809 Stress-Induced RNA Granulation. *Mol Cell,* **70**, 175-187 e178.

810 Neumann, M., Kwong, L.K., Lee, E.B., Kremmer, E., Flatley, A., Xu, Y., Forman, M.S., Troost, D.,
811 Kretzschmar, H.A., Trojanowski, J.Q., et al. (2009). Phosphorylation of S409/410 of TDP-43
812 is a consistent feature in all sporadic and familial forms of TDP-43 proteinopathies. Acta
813 Neuropathol 117, 137-149.

814 Neumann, M., Sampathu, D.M., Kwong, L.K., Truax, A.C., Micsenyi, M.C., Chou, T.T., Bruce, J.,
815 Schuck, T., Grossman, M., Clark, C.M. et al. (2006) Ubiquitinated TDP-43 in frontotemporal
816 lobar degeneration and amyotrophic lateral sclerosis. *Science,* **314**, 130-133.

817 Nishimoto, Y., Nakagawa, S., Hirose, T., Okano, H.J., Takao, M., Shibata, S., Suyama, S.,
818 Kuwako, K., Imai, T., Murayama, S. et al. (2013) The long non-coding RNA nuclear-enriched
819 abundant transcript 1_2 induces paraspeckle formation in the motor neuron during the early
820 phase of amyotrophic lateral sclerosis. *Mol Brain,* **6**, 31.

821 Patel, A., Lee, H.O., Jawerth, L., Maharana, S., Jahnel, M., Hein, M.Y., Stoynov, S., Mahamid, J.,
822 Saha, S., Franzmann, T.M. et al. (2015) A Liquid-to-Solid Phase Transition of the ALS
823 Protein FUS Accelerated by Disease Mutation. *Cell,* **162**, 1066-1077.

824 Polymenidou, M., Lagier-Tourenne, C., Hutt, K.R., Huelga, S.C., Moran, J., Liang, T.Y., Ling,
825 S.C., Sun, E., Wancewicz, E., Mazur, C., et al. (2011). Long pre-mRNA depletion and RNA
826 missplicing contribute to neuronal vulnerability from loss of TDP-43. Nat Neurosci 14,
827 459-468.

828 Qamar, S., Wang, G., Randle, S.J., Ruggeri, F.S., Varela, J.A., Lin, J.Q., Phillips, E.C., Miyashita,
829 A., Williams, D., Strohl, F. et al. (2018) FUS Phase Separation Is Modulated by a Molecular
830 Chaperone and Methylation of Arginine Cation-pi Interactions. *Cell,* **173**, 720-734 e715.

831 Ramaswami, M., Taylor, J.P. and Parker, R. (2013) Altered ribostasis: RNA-protein granules in
832 degenerative disorders. *Cell,* **154**, 727-736.

833 Ratti, A. and Buratti, E. (2016) Physiological functions and pathobiology of TDP-43 and FUS/TLS
834 proteins. *J Neurochem,* **138 Suppl 1**, 95-111.

835 Ryan, V.H., Dignon, G.L., Zerze, G.H., Chabata, C.V., Silva, R., Conicella, A.E., Amaya, J.,
836 Burke, K.A., Mittal, J. and Fawzi, N.L. (2018) Mechanistic View of hnRNPA2
837 Low-Complexity Domain Structure, Interactions, and Phase Separation Altered by Mutation
838 and Arginine Methylation. *Molecular Cell,* **69**, 465-479.e467.

839 Santama, N., Ogg, S.C., Malekkou, A., Zographos, S.E., Weis, K., and Lamond, A.I. (2005).
840 Characterization of hCINAP, a novel coilin-interacting protein encoded by a transcript from
841 the transcription factor TAFIID32 locus. The Journal of biological chemistry 280,
842 36429-36441.

843 Schirmer, L., Velmeshev, D., Holmqvist, S., Kaufmann, M., Werneburg, S., Jung, D., Vistnes, S.,
844 Stockley, J.H., Young, A., Steindel, M. et al. (2019) Neuronal vulnerability and multilineage
845 diversity in multiple sclerosis. *Nature*, [Epub ahead of print].

846 Schmidt, H.B., and Rohatgi, R. (2016). In Vivo Formation of Vacuolated Multi-phase
847 Compartments Lacking Membranes. *Cell Rep,* **16**, 1228-1236.

848 Shevtsov, S.P. and Dundr, M. (2011) Nucleation of nuclear bodies by RNA. *Nat Cell Biol,* **13**,
849 167-173.

850 Stanek, D. and Fox, A.H. (2017) Nuclear bodies: news insights into structure and function. *Curr*
851 *Opin Cell Biol,* **46**, 94-101.

852 Sun, X., Duan, Y., Qin, C., Li, J.C., Duan, G., Deng, X., Ni, J., Cao, X., Xiang, K., Tian, K., Chen,
853 C.H., Li, A., and Fang, Y. (2018) Distinct multilevel misregulations of Parkin and PINK1
854 revealed in cell and animal models of TDP-43 proteinopathy. *Cell Death Dis*, **9**, 953.

855 Taylor, J.P., Brown, R.H., Jr. and Cleveland, D.W. (2016) Decoding ALS: from genes to
856 mechanism. *Nature,* **539**, 197-206.

857 Udan-Johns, M., Bengoechea, R., Bell, S., Shao, J., Diamond, M.I., True, H.L., Weihl, C.C. and
858 Baloh, R.H. (2014) Prion-like nuclear aggregation of TDP-43 during heat shock is regulated
859 by HSP40/70 chaperones. *Hum Mol Genet,* **23**, 157-170.

860 Ukmar-Godec, T., Hutten, S., Grieshop, M.P., Rezaei-Ghaleh, N., Cima-Omori, M.S., Biernat, J.,
861 Mandelkow, E., Soding, J., Dormann, D., and Zweckstetter, M. (2019).
862 Lysine/RNA-interactions drive and regulate biomolecular condensation. Nat Commun 10,
863 2909.

864 Uversky, V.N. (2017) Intrinsically disordered proteins in overcrowded milieu: Membrane-less
865 organelles, phase separation, and intrinsic disorder. *Curr Opin Struct Biol,* **44**, 18-30.

866 Valgardsdottir, R., Chiodi, I., Giordano, M., Cobianchi, F., Riva, S. and Biamonti, G. (2005)
867 Structural and Functional Characterization of Noncoding Repetitive RNAs Transcribed in
868 Stressed Human Cells. *Molecular Biology of the Cell,* **16**, 2597-2604.

869 van Es, M.A., Hardiman, O., Chio, A., Al-Chalabi, A., Pasterkamp, R.J., Veldink, J.H. and van
870 den Berg, L.H. (2017) Amyotrophic lateral sclerosis. *The Lancet,* **390**, 2084-2098.

871 Wang, L., Kang, J., Lim, L., Wei, Y. and Song, J. (2018) TDP-43 NTD can be induced while CTD
872 is significantly enhanced by ssDNA to undergo liquid-liquid phase separation. *Biochem*
873 *Biophys Res Commun,* **499**, 189-195.

874 Wang, Y., Hu, S.B., Wang, M.R., Yao, R.W., Wu, D., Yang, L. and Chen, L.L. (2018)
875 Genome-wide screening of NEAT1 regulators reveals cross-regulation between
876 paraspeckles and mitochondria. *Nat Cell Biol*, **20**, 1145-1158.

877 Wegener, M. and Muller-McNicoll, M. (2018) Nuclear retention of mRNAs - quality control, gene
878 regulation and human disease. *Semin Cell Dev Biol,* **79**, 131-142.

879 West, J.A., Mito, M., Kurosaka, S., Takumi, T., Tanegashima, C., Chujo, T., Yanaka, K., Kingston,
880 R.E., Hirose, T., Bond, C., et al. (2016) Structural, super-resolution microscopy analysis of
881 paraspeckle nuclear body organization. *J Cell Biol*, **214**, 817-830.

882 Xiang, S., Kato, M., Wu, L.C., Lin, Y., Ding, M., Zhang, Y., Yu, Y. and McKnight, S.L. (2015) The
883 LC Domain of hnRNPA2 Adopts Similar Conformations in Hydrogel Polymers, Liquid-like
884 Droplets, and Nuclei. *Cell,* **163**, 829-839.

885 Yamazaki, T., Souquere, S., Chujo, T., Kobelke, S., Chong, Y.S., Fox, A.H., Bond, C.S.,
886 Nakagawa, S., Pierron, G. and Hirose, T. (2018) Functional Domains of NEAT1
887 Architectural lncRNA Induce Paraspeckle Assembly through Phase Separation. *Molecular*
888 *Cell,* **70**, 1038-1053.e1037.

889 Zhao, M., Kim, J.R., van Bruggen, R. and Park, J. (2018) RNA-Binding Proteins in Amyotrophic
890 Lateral Sclerosis. *Mol Cells,* **41**, 818-829.

891 **FIGURE LEGENDS**

892 **Figure 1. TDP-43 forms reversible, dynamic NBs in response to arsenic stress.**
893 (**A**) Representative confocal images of HeLa cells in the absence (PBS) or presence of arsenite
894 (250 μM, 30 min) forming TDP-43 NBs (arrows) and TDP-43$^+$ SGs (arrowheads) (also see Movie
895 S1). All cells are transfected with TDP-43-HA (anti-HA) and stained for SGs with anti-TIAR;
896 merged images with DAPI staining for DNA (blue) are shown. Arrows, TDP-43 NBs; arrowheads,
897 SGs associated with TDP-43 (TDP-43$^+$ SGs). (**B**) Quantification of the percentage of cells that
898 show TDP-43 NBs or TDP-43$^+$ SGs before and after arsenite the treatment in (A). (**C**)
899 Representative images of the NBs formed by endogenous TDP-43 (enTDP-43) in HeLa cells
900 upon arsenite treatment. (**D-E**) Quantifications of the percentage of cells in (C) showing
901 stress-induced enTDP-43 NBs (D) and the size (μm^2) of the NBs (E). (**F-G**) Representative
902 images of the FRAP analysis of GFP-TDP-43 NBs in *live* cells after arsenite treatment for 30 min
903 (F) (also see Video S2) or 6 h (G). (**H**) The FRAP recovery curves of (F and G) are quantified by
904 averaging the relative fluorescence intensity (FI) of TDP-43 NBs of similar size at indicated time.
905 The relative FI of each TDP-43 NB prior to photobleaching is set to 100% and the time 0 refers to
906 the time point right after photobleaching. (**I**) Representative images showing the disappearance
907 of TDP-43 NBs and TDP-43$^+$ SGs after arsenite washout. (**J-L**) Quantification of the percentage
908 of cells showing TDP-43$^+$ SGs (J), TDP-43 NBs (K) or the average count of TDP-43 NBs per cell
909 (L) at indicated time points after arsenite washout in (I). Data are shown as mean ± SEM, except
910 for (E) and (L) box-and-whisker plots with the value of each data measured. n = ~100 cells for
911 each group in (B, D-E, J-K), n = 9 in (H), and n = ~15 cells for each group in (L), pooled results
912 from 3 independent repeats. Statistic significance is determined at *$p < 0.05$, **$p < 0.01$, ***$p <$
913 0.001 by Student's *t*-test for comparison between PBS and arsenite within the same group and
914 two-way ANOVA for comparison of the stress-induced changes between different groups in (B)
915 Student's *t*-test in (D), two-way ANOVA in (H), and one-way ANOVA in (J-L). Scale bars, 10 μm
916 in (A) and 5 μm in (C, F, G and I).
917

918 **Figure 2. Inhibition of nuclear export induces the assembly of TDP-43 NBs.**

919 (**A-B**) Representative images of endogenous TDP-43 (enTDP-43) forming NBs upon LMB
920 treatment (25 nM, 18 h). Percentage of cells showing distinct TDP-43 NBs in (A) is quantified in
921 (B). (**C**) A diagram showing the major domains of human TDP-43 and the residues mutated in
922 the localization signals. NLS, nuclear localization signal; RRM, RNA recognition motif; NES,
923 nuclear export signal; LCD, low complexity domain. (**D**) Representative images of 293T cells
924 transfected with WT, NLS^{mut} or NES^{mut} TDP-43. (**E-F**) The percentage of cells with NBs (E) and
925 the average number of NBs per cell (F) are quantified. (**G-H**) Representative Western blot
926 images (G) and quantifications (H) of WT, NLS^{mut} and NES^{mut} TDP-43 proteins in the soluble (S,
927 supernatants in RIPA) and insoluble fractions (I, pellets resuspended in 9 M of urea). Mean ±
928 SEM, except for (F) box-and-whisker plots. n = ~120 in (B, E) and ~10 cells in (F) for cells each
929 condition or group from pooled results of 3 independent repeats, n = 3 in (G, H); $*p < 0.05$, $**p <$
930 0.01, $***p < 0.001$; ns, not significant; Student's *t*-test in (B), one-way ANOVA in (E, F, H). Scale
931 bar: 5 μm.

932

933 **Figure 3. Formation of NBs mitigates TDP-43-mediated cytotoxicity.**

934 (**A**) OE of the WT or NLS^{mut} but not NES^{mut} TDP-43 in 293T cells decreases the cell viability,
935 measured by a CCK-8 assay. (**B**) The relative ATP levels of the 293T cells transfected of WT,
936 NLS^{mut} or NES^{mut} TDP-43 measured using a CellTiter-Glo® luminescent assay. (**C-D**) Diagrams
937 showing the K145/192Q mutation in the WT TDP-43 and the K145/192R mutation in the NES^{mut}
938 TDP-43, respectively. (**E-F'**) Representative confocal images of the WT (E) and "WT +
939 K145/192Q" TDP-43 (E'), or the NES^{mut} (F) and "NES^{mut} + K145/192R" TDP-43 (F') in 293T cells.
940 (**G-H**) Quantifications of the average numbers of TDP-43 NBs per cell formed in each group in
941 (E-F') as indicated. (**I-J**) Percentages of cells with TDP-43 exclusively in the nucleus (nuc) or in
942 both the nucleus and the cytoplasm (cyto) in (E-F') are quantified. (**K-L**) The viability of cells
943 expressing the WT or NES^{mut} TDP-43 with the indicated NB-promoting or NB-suppressing
944 mutation is assessed using the CCK-8 assay. Mean ± SEM, except for (G-H) box-and-whisker

945 plots; n = 3~4 in (A-B, K-L), n = ~12 cells in (G-H) and over 100 cells in (I-J) for each group from
946 pooled results of 3 independent repeats; *p < 0.05, **p < 0.01, ***p < 0.001; ns, not significant;
947 one-way ANOVA in (A-B), Student's *t*-test in (G-H, K-L), two-way ANOVA in (I-J). Scale bar: 5
948 μm.
949

950 **Figure 4. The RRM1 and RRM2 function complementarily to maintain the core-shell**
951 **organization of TDP-43 NBs.**

952 (**A**) A diagram showing the major functional domains of WT TDP-43 and the ΔRRM1 and
953 ΔRRM2 mutants. (**B**) LIGHTNING super-resolution microscopy of 293T cells transfected with
954 Myc-TDP-43-WT, ΔRRM1 or ΔRRM2 and treated with LMB. Higher magnification images
955 (zoom-ins) and 3D renderings of the boxed areas are shown. (**C**) The average diameters of the
956 WT, ΔRRM1 and ΔRRM2 TDP-43 nuclear structures in (B) are quantified. (**D**) A schematic
957 model of the core-shell organization of TDP-43 NBs (red) and the distinct distribution of ΔRRM1
958 (green) and ΔRRM2 (blue). (**E-H**) LIGHTNING multicolor super-resolution microscopy and higher
959 magnification images of representative LMB-induced TDP-43 NBs. Cells are co-transfected with
960 a combination of HA- or Myc-tagged WT, ΔRRM1 or ΔRRM2 TDP-43 as indicated. (**I-P**) The
961 intensity profiles (I-L) along the indicated lines and the average diameters (M-P) of TDP-43 NBs
962 in each group are shown. (**Q-S**) Representative super-resolution microscopy images and the
963 intensity line analyses of WT (Q), ΔRRM1 (R) or ΔRRM2 (S) TDP-43 nuclear structures (green)
964 co-immunostained with the paraspeckle protein NONO (purple) are shown. The box-and-whisker
965 plots with the value of each NB measured are shown. n = ~900 NBs in (C, M-P) for each group
966 from pooled results of at least 3 independent repeats; $^{\#}p$ < 0.0001; one-way ANOVA in (C) and
967 Student's *t*-test in (M-P). Scale bars: 5 μm in (B), 2 μm in (E-H), 200 nm in the zoom-ins, and 500
968 nm in (Q-S).
969

970 **Figure 5. *NEAT1* RNA promotes TDP-43 LLPS *in vitro* and is upregulated in stressed**
971 **neurons**

972 (**A**) A diagram showing the WT, ΔRRM1 and ΔRRM2 of TDP-43$^{1-274}$. (**B-K)** The total RNA
973 extracts (B-D), tRNA (E-G), or lncRNA *NEAT1* (I-K) are added into the *in vitro* LLPS assay of WT,
974 ΔRRM1 and ΔRRM2 TDP-43$^{1-273}$ as indicated. C', a higher concentration of ΔRRM1 is also
975 included in order to start the suppression assay with large LDs as those of WT TDP-43. H,
976 representative images of the *in vitro* dot-blot assay confirming direct binding of *NEAT1* RNA to
977 TDP-43 protein. The bound RNA is visualized using the SYBR® Gold Nucleic Acid Gel Stain kit
978 and the protein loaded is stained by Ponceau S. Bovine serum albumin (BSA) is used as a
979 negative binding control. (**L-N**) tRNA-mediated suppression of TDP-43 LLPS can be antagonized
980 by increasing the level of *NEAT1* RNA. The concentrations of NaCl, the crowding agent PEG,
981 TDP-43 proteins and RNAs used in the *in vitro* assays are indicated. (**O-Q'**) Representative
982 images of primary mouse cortical neurons infected with WT (O-O'), ΔRRM1 (P-P') and ΔRRM2
983 (Q-Q') TDP-43 treated with PBS or arsenite as indicated. TDP-43-HA (green), microtubule
984 associated protein 2 (MAP2) to mark neuronal perikarya and dendrites (red), and merged
985 images with DAPI staining to label the nucleus (blue). Zoom-in images of the boxed areas are
986 shown. (**R-T**) Higher magnification images and the intensity line analyses of the nuclear
987 structures pointed by the arrows in O'-Q' are shown. (**U**) The percentage of primary mouse
988 neurons forming WT TDP-43 NBs in response to arsenic stress in (O-O') is quantified. (**V-W**)
989 Cellular stress induced by arsenite (V) or LMB (W) increases the levels of both total *NEAT1* RNA
990 and the *NEAT1_2* isoform in mouse primary neurons compared to the vehicle control. Mean ±
991 SEM; n = ~100 cells each group from pooled results of 3 independent repeats in (U), n = 3 in
992 (V-W); *$p < 0.05$, **$p < 0.01$, ***$p < 0.001$; Student's *t*-test. Scale bars: 2 μm in (B-G, I-N), 5 μm in
993 (O-Q') and 2 μm in the zoom-ins.
994

995 **Figure 6. TDP-43-D169G impairs NB assembly, accumulates pathological cytoplasmic**
996 **foci and potentiates the cytotoxicity of TDP-43 in prolonged stress and during aging.**
997 (**A**) A diagram showing WT and D169G mutant TDP-43. (**B**) Representative Western blot image
998 and quantification confirming the expression levels of WT and D169G TDP-43 in HeLa cells. (**C**)

999 Representative confocal images of HeLa cells transfected with WT or D169G TDP-43, treated
1000 with arsenite for 0 min (PBS), 30 min or 120 min as indicated. Green, TDP-43-HA (anti-HA); Red,
1001 anti-G3BP for SGs; Blue, DAPI staining for DNA (nucleus). (**D-F**) The percentage of cells with
1002 TDP-43 NBs (D), the average count of TDP-43 NBs per cell (E) and the percentage of cells with
1003 TDP-43$^+$ SGs (F) at indicated time after arsenite treatment in (C). (**G-H**) Confocal images of
1004 representative single cells expressing WT (G) or D169G TDP-43-HA (H) that form cytoplasmic
1005 foci (green) after arsenite treatment for 6 h were co-stained for pS409/410 (red) and DAPI for
1006 DNA (blue). Higher magnification images of the boxed areas are shown on the side. (**I**) The
1007 percentage of cells with pS409/10$^+$ TDP-43 cytoplasmic foci at indicated times during prolonged
1008 stress (arsenite, 250 μM) is quantified. Arrows, TDP-43 NBs; arrowheads, TDP-43$^+$ SGs;
1009 asterisks, pTDP-43$^+$ cytoplasmic foci. (**J-K**) Representative images (J) and quantification (K) of
1010 PI staining to evaluate the death of cells expressing WT or D169G TDP-43. (**L-M**)
1011 Representative images (L) and quantification (M) of the Western blot analysis confirming the
1012 expression levels and solubility of hTDP-43-D169G in the transgenic flies. (**N**) Representative
1013 z-stack images of the fly eye (driven by a GMR-Gal4 driver) expressing WT or D169G hTDP-43
1014 at indicated time points. The degeneration severity is assessed by the rough surface, swelling
1015 and loss of pigment cells of the compound eyes. The average degeneration score (mean ± SEM)
1016 and the statistic significance (compared to the UAS-*lacZ* control flies) are indicated at the bottom
1017 of each group. (**O**) The climbing capability of the flies expressing WT or D169G hTDP-43 in
1018 motor neurons (D42-Gal4) is evaluated as percentage of flies climbing over 3 cm in 10 seconds.
1019 The UAS-*luciferase* fly line is used as a control. The numbers of flies tested in each group are
1020 indicated. Mean ± SEM, except for (E) box-and-whisker plots; n = 3 in (B, M), n = ~100 cells in (D,
1021 F, I), ~8 cells in (E) and ~2000 cells in (K) for each group from pooled results of 3 independent
1022 repeats, n = 13~16 eyes each group in (N); *$p < 0.05$, **$p < 0.01$, ***$p < 0.001$; ns, not significant;
1023 Student's *t*-test in (B, E, K, M), one-way ANOVA in (N) and two-way ANOVA in (D, F, I, O). Scale
1024 bars: 5 μm in (C, G-H), 50 μm in (J) and 100 μm in (N).
1025

1026 **Figure 7. *NEAT1*-mediated nucleation of TDP-43 droplets *in vitro* and in stressed cells is**
1027 **impaired by the D169G mutation.**
1028 (**A-B**) Both WT and D169G TDP-43 form LDs by LLPS in a dose-dependent manner. (**C-D**)
1029 Suppression of the *in vitro* LLPS of WT and D169G TDP-43 by total RNA extracts. (**E-F**)
1030 Promotion of TDP-43 LLPS by *NEAT1* RNA is dramatically reduced in the D169G TDP-43. The
1031 concentrations of NaCl, TDP-43, PEG and RNA used in the *in vitro* assays are as indicated. (**G-H**)
1032 The representative EMSA image (G) and quantification (H) of the gel shifts of *NEAT1* RNA (2 ug)
1033 incubated with indicated concentrations of WT or D169G TDP-43$^{1-274}$ protein. All shifts are shown
1034 as percentage of the distance the control *NEAT1* RNA band migrates (0 μM protein). (**I-L**)
1035 Representative confocal images of WT (I-J) or D169G (K-L) TDP-43 NBs induced by arsenite
1036 treatment (250 μM, 30 min) compared to the vehicle control (PBS) in HeLa cells. The cells are
1037 co-stained for *NEAT1* lncRNA by FISH using a probe that target the middle sequence of
1038 *NEAT1_2*. Higher magnification images of the boxed areas are shown on the side. (**M-P**) For the
1039 colocalization analysis of the entire cell, the fluorescence intensity of TDP-43-HA and *NEAT1*
1040 lncRNA of each pixel in the cells in (I-L) is measured and plotted. Pearson's correlation
1041 coefficient is used as a measure of colocalization. The mean correlation coefficient value ± SEM
1042 of ~20 cells per group is shown at the bottom of each representative plot. (**Q-R**) The knockdown
1043 efficiency of the siRNA against *NEAT1* (si*NEAT1*) is determined by qPCR. Both total *NEAT1*
1044 RNA (Q) and the *NEAT1_2* isoform (R) are examined. (**S-W**) Representative confocal images
1045 (S-U) and quantifications (V-W) of stress-induced *NEAT1* puncta (V) or TDP-43 NBs in cells
1046 treated with scramble siRNA (si*Ctrl*) or si*NEAT1*. Mean ± SEM, n = 4 in (G, Q-R), n = ~10 cells
1047 each group from pooled results of 3 independent repeats in (V-W); *$p < 0.05$, **$p < 0.01$, ***$p <$
1048 0.001; ns, not significant; two-way ANOVA in (H), Student's *t*-test in (M, R, V, W). Scale bars: 2
1049 μm in (A-F) and 5 μm in (I-L, S-U).

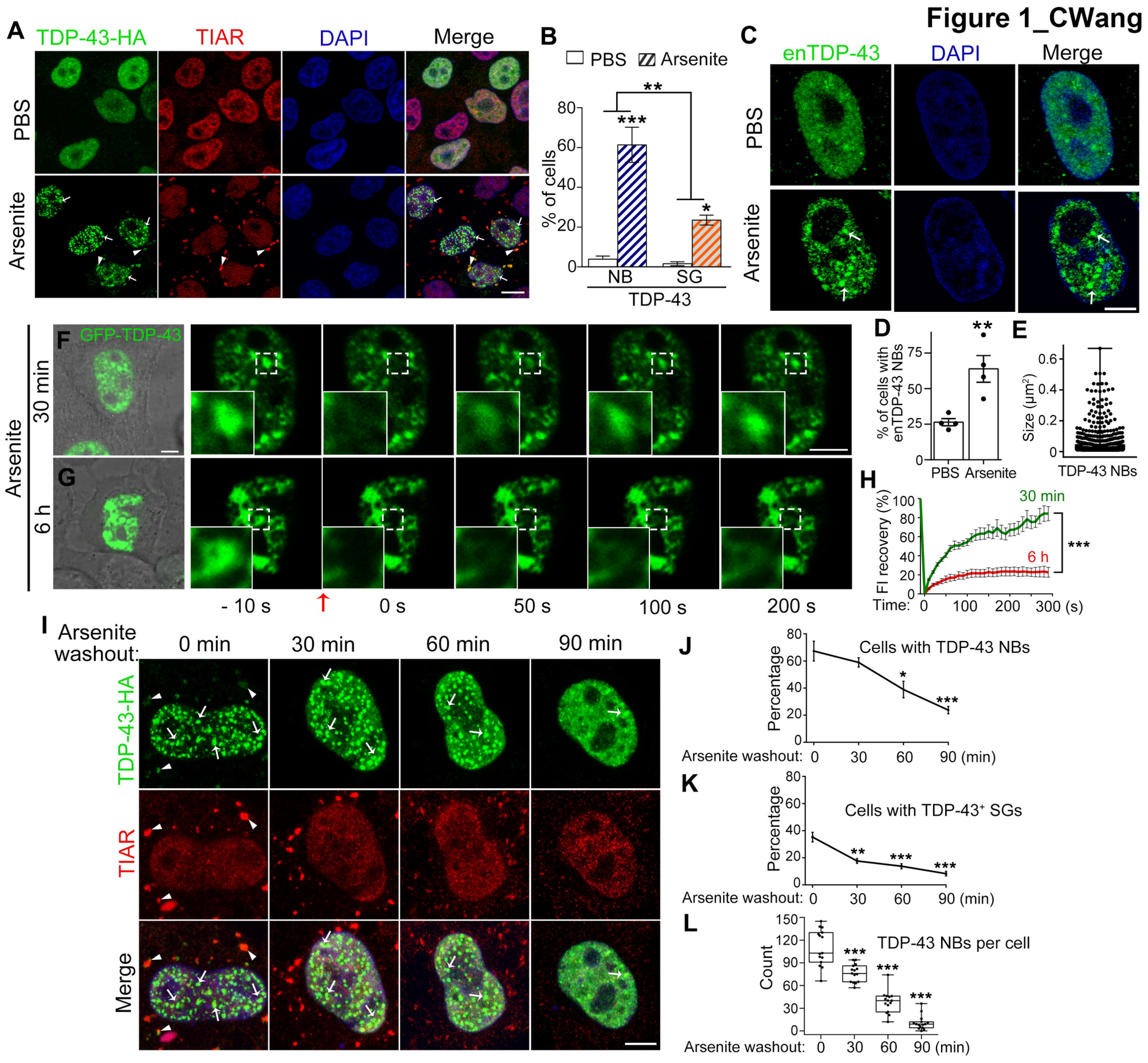
Figure 1_CWang
A
TDP-43-HA
TIAR
DAPI
Merge
PBS
Arsenite
B
PBS
Arsenite
% of cells
NB
SG
TDP-43
C
enTDP-43
DAPI
Merge
PBS
Arsenite
D
% of cells with enTDP-43 NBs
PBS
Arsenite
E
Size (μm²)
TDP-43 NBs
F
GFP-TDP-43
30 min
G
6 h
Arsenite
- 10 s
0 s
50 s
100 s
200 s
H
FI recovery (%)
30 min
6 h
Time:
(s)
I
Arsenite washout:
0 min
30 min
60 min
90 min
TDP-43-HA
TIAR
Merge
J
Cells with TDP-43 NBs
Percentage
Arsenite washout:
(min)
K
Cells with TDP-43⁺ SGs
Percentage
Arsenite washout:
(min)
L
TDP-43 NBs per cell
Count
Arsenite washout:
(min)

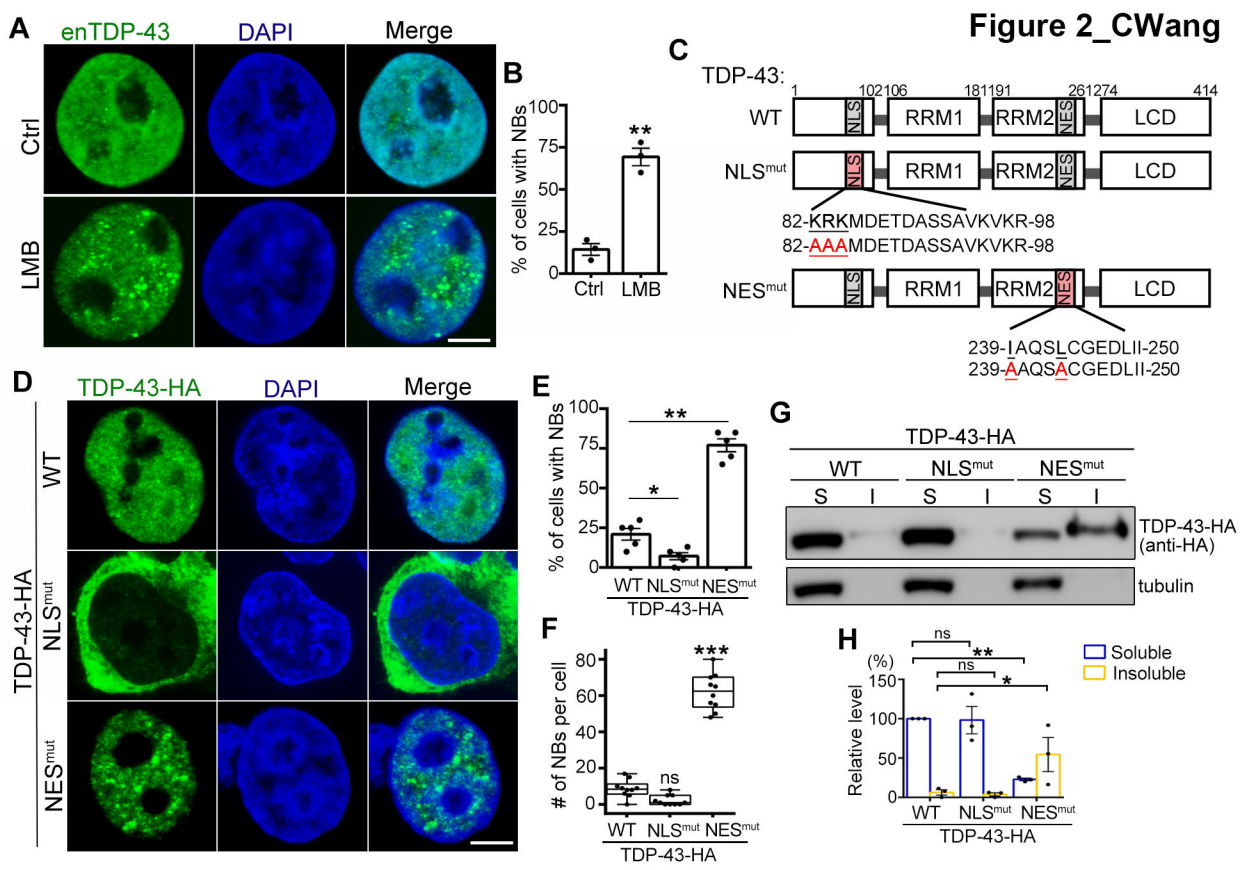
Figure 2_CWang
A
enTDP-43
DAPI
Merge
Ctrl
LMB
B
% of cells with NBs
100
75
50
25
0
**
Ctrl
LMB
C
TDP-43:
1
102
106
181
191
261
274
414
WT
NLS
RRM1
RRM2
NES
LCD
NLSmut
82-KRKMDETDASSAVKVKR-98
82-AAAMDETDASSAVKVKR-98
NESmut
239-IAQSLCGEDLII-250
239-AAQSACGEDLII-250
D
TDP-43-HA
DAPI
Merge
TDP-43-HA
WT
NLSmut
NESmut
E
% of cells with NBs
100
75
50
25
0
**
*
WT
NLSmut
NESmut
TDP-43-HA
F
# of NBs per cell
80
60
40
20
0
***
ns
WT
NLSmut
NESmut
TDP-43-HA
G
TDP-43-HA
WT
NLSmut
NESmut
S
I
S
I
S
I
TDP-43-HA
(anti-HA)
tubulin
H
(%)
Relative level
150
100
50
0
ns
**
ns
*
Soluble
Insoluble
WT
NLSmut
NESmut
TDP-43-HA

Figure 3_CWang

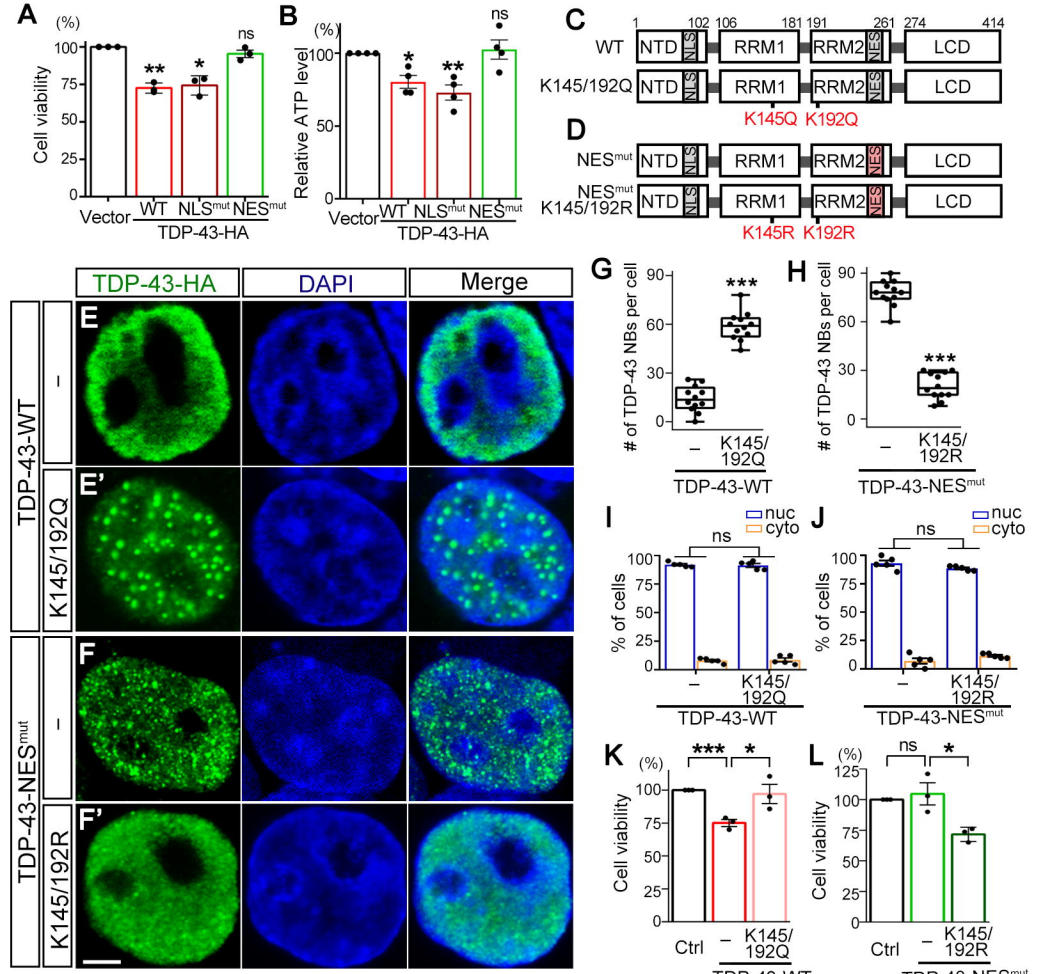

Figure 4_CWang

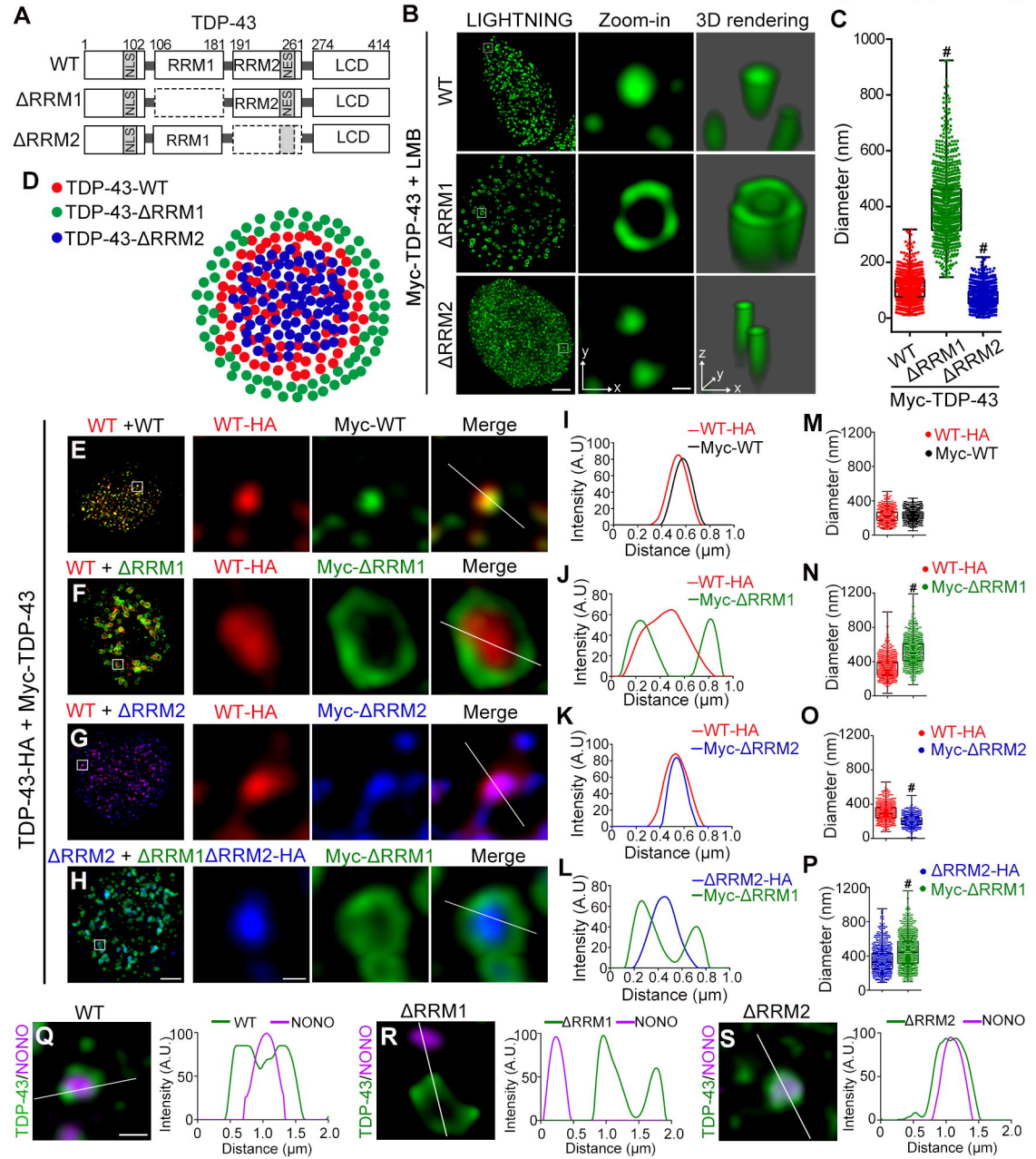

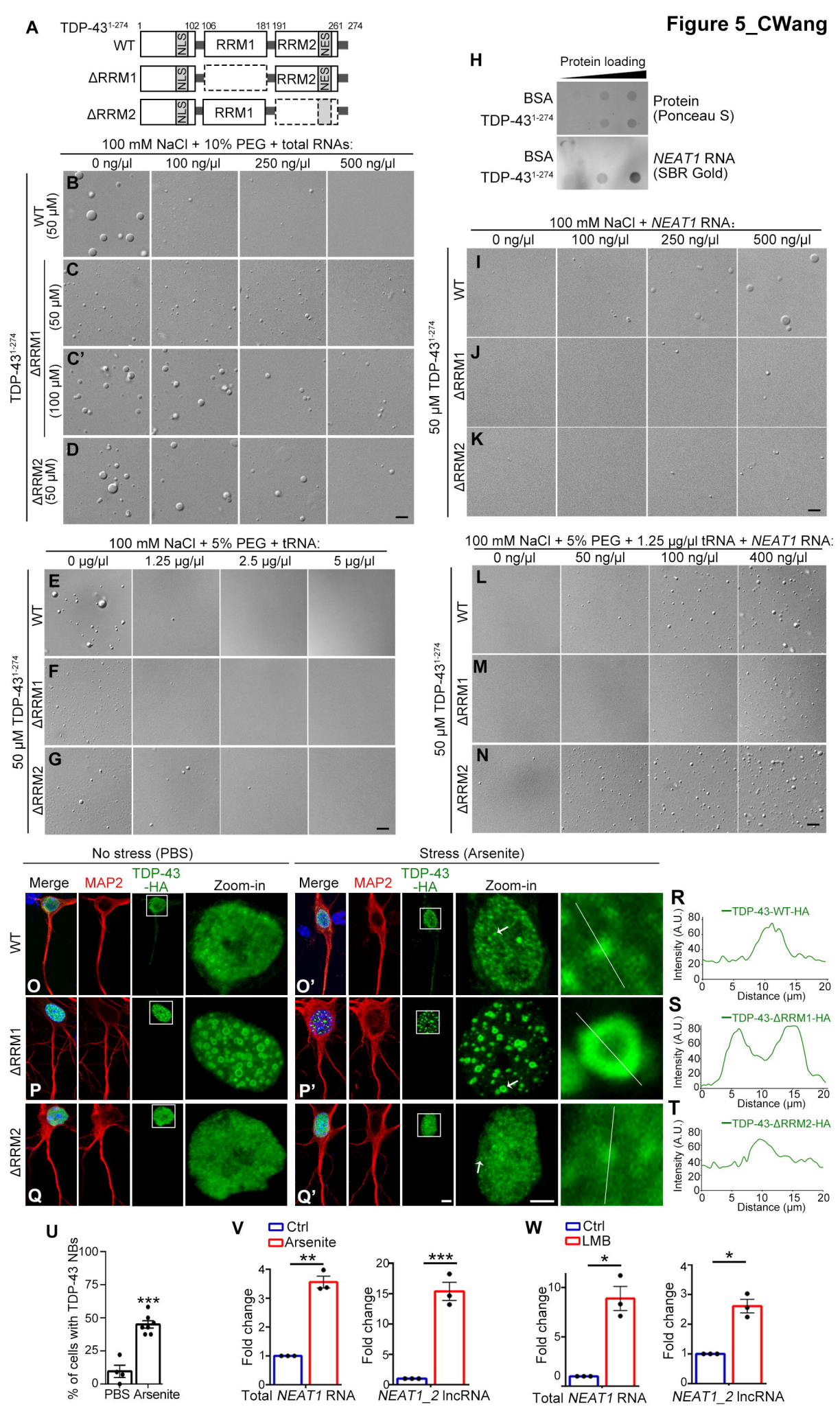
Figure 5_CWang
A
TDP-43 1-274
1
102
106
181
191
261
274
WT
NLS
RRM1
RRM2
NES
ΔRRM1
ΔRRM2
100 mM NaCl + 10% PEG + total RNAs:
0 ng/μl
100 ng/μl
250 ng/μl
500 ng/μl
B
C
C'
D
WT (50 μM)
ΔRRM1 (50 μM)
(100 μM)
ΔRRM2 (50 μM)
H
Protein loading
BSA
TDP-43 1-274
Protein (Ponceau S)
NEAT1 RNA (SBR Gold)
100 mM NaCl + NEAT1 RNA:
I
J
K
50 μM TDP-43 1-274
100 mM NaCl + 5% PEG + tRNA:
0 μg/μl
1.25 μg/μl
2.5 μg/μl
5 μg/μl
E
F
G
100 mM NaCl + 5% PEG + 1.25 μg/μl tRNA + NEAT1 RNA:
0 ng/μl
50 ng/μl
100 ng/μl
400 ng/μl
L
M
N
No stress (PBS)
Stress (Arsenite)
Merge
MAP2
TDP-43 -HA
Zoom-in
O
P
Q
O'
P'
Q'
R
S
T
TDP-43-WT-HA
TDP-43-ΔRRM1-HA
TDP-43-ΔRRM2-HA
Intensity (A.U.)
Distance (μm)
U
% of cells with TDP-43 NBs
PBS
Arsenite
V
Ctrl
Arsenite
Fold change
Total NEAT1 RNA
NEAT1_2 lncRNA
W
Ctrl
LMB

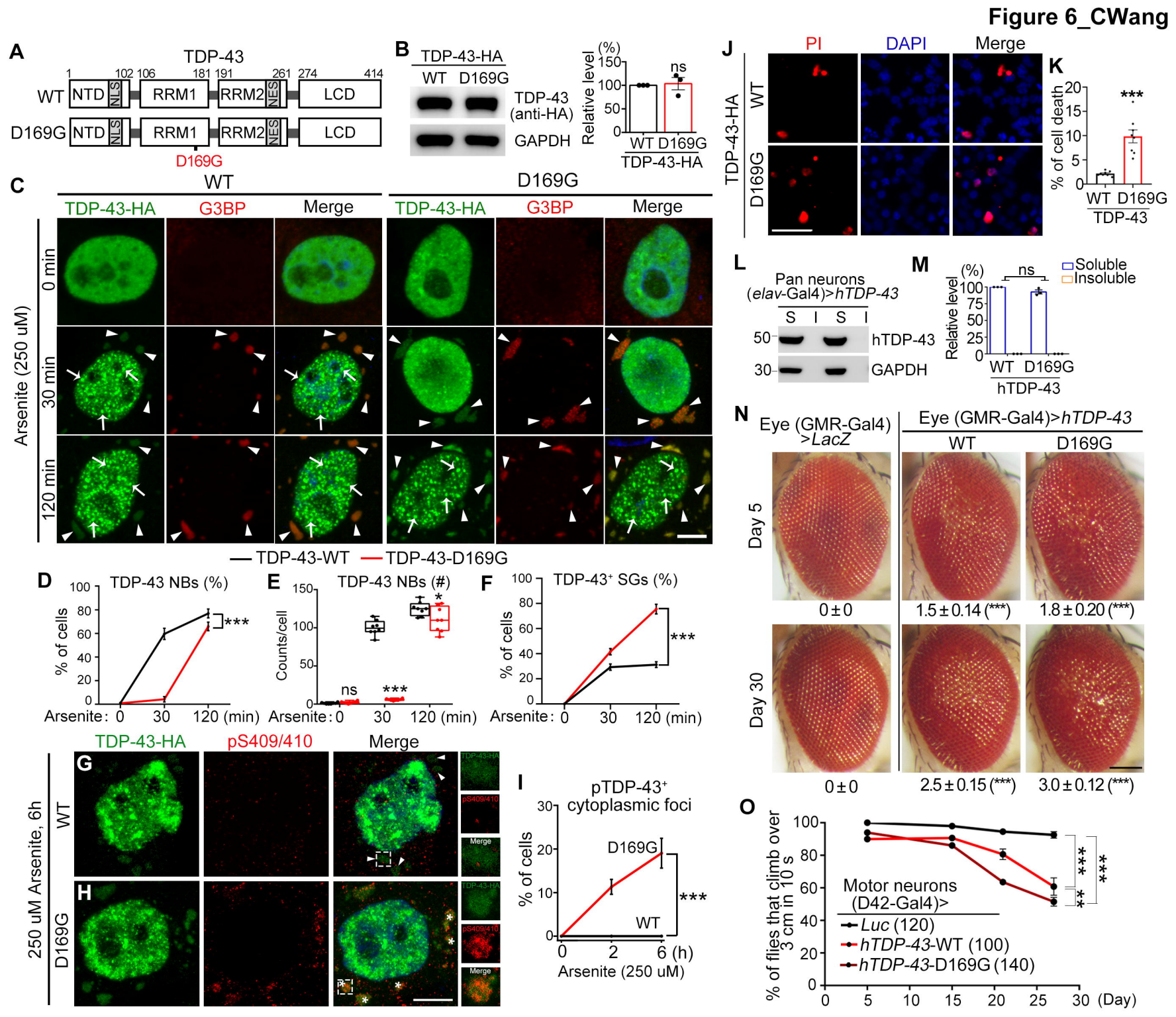
A
TDP-43
1 102 106 181 191 261 274 414
WT NTD NLS RRM1 RRM2 NES LCD
D169G NTD NLS RRM1 RRM2 NES LCD
D169G
B
TDP-43-HA
WT D169G
TDP-43 (anti-HA)
GAPDH
Relative level (%)
ns
WT D169G
TDP-43-HA
C
WT
D169G
TDP-43-HA G3BP Merge
Arsenite (250 uM)
0 min
30 min
120 min
TDP-43-WT TDP-43-D169G
D
TDP-43 NBs (%)
% of cells
Arsenite: 0 30 120 (min)
E
TDP-43 NBs (#)
Counts/cell
ns ***
F
TDP-43+ SGs (%)
% of cells
G
H
TDP-43-HA pS409/410 Merge
250 uM Arsenite, 6h
WT
D169G
I
pTDP-43+ cytoplasmic foci
% of cells
D169G
WT
Arsenite (250 uM)
J
PI DAPI Merge
TDP-43-HA
WT
D169G
K
% of cell death
WT D169G
TDP-43
L
Pan neurons (elav-Gal4)>hTDP-43
S I S I
hTDP-43
GAPDH
M
Soluble
Insoluble
Relative level (%)
ns
WT D169G
hTDP-43
N
Eye (GMR-Gal4) >LacZ
Eye (GMR-Gal4)>hTDP-43
WT D169G
Day 5
Day 30
0 ± 0
1.5 ± 0.14 (***)
1.8 ± 0.20 (***)
0 ± 0
2.5 ± 0.15 (***)
3.0 ± 0.12 (***)
O
% of flies that climb over 3 cm in 10 s
Motor neurons (D42-Gal4)>
Luc (120)
hTDP-43-WT (100)
hTDP-43-D169G (140)
(Day)

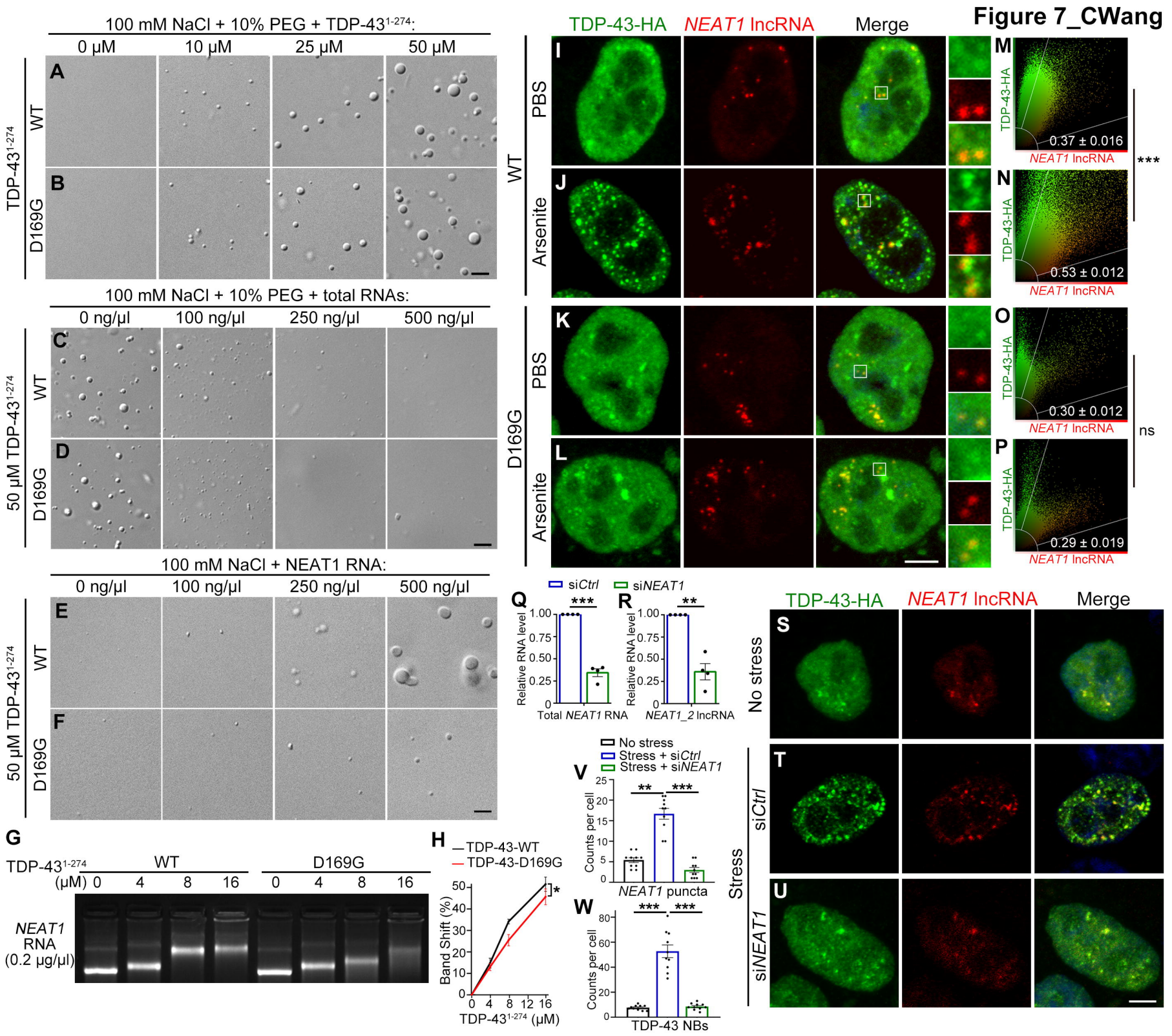

Figure 7_CWang
100 mM NaCl + 10% PEG + TDP-43 1-274:
0 μM
10 μM
25 μM
50 μM
TDP-43 1-274
WT
D169G
A
B
100 mM NaCl + 10% PEG + total RNAs:
0 ng/μl
100 ng/μl
250 ng/μl
500 ng/μl
50 μM TDP-43 1-274
C
D
100 mM NaCl + NEAT1 RNA:
E
F
TDP-43-HA
NEAT1 lncRNA
Merge
PBS
Arsenite
I
J
K
L
M
N
O
P
0.37 ± 0.016
0.53 ± 0.012
0.30 ± 0.012
0.29 ± 0.019
***
ns
siCtrl
siNEAT1
Q
R
Relative RNA level
Total NEAT1 RNA
NEAT1_2 lncRNA
No stress
Stress + siCtrl
Stress + siNEAT1
V
W
Counts per cell
NEAT1 puncta
TDP-43 NBs
S
T
U
Stress
G
TDP-43 1-274
(μM)
0
4
8
16
NEAT1 RNA (0.2 μg/μl)
H
TDP-43-WT
TDP-43-D169G
Band Shift (%)
TDP-43 1-274 (μM)